國立臺灣大學醫學院藥理學研究所

碩士論文

Graduate Institute of Pharmacology
College of Medicine
National Taiwan University

Master Thesis

探討 FGFR 介導 TGFβR 訊息如何調控 Fibroblast 分化成 Adipocyte 或 Myofibroblast 的機制

FGFR Mediates TGFβR Signaling to Switch Fibroblast Differentiation between Adipocytes and Myofibroblasts

洪堂萌

Tang-Meng Hong

指導老師：蔡丰喬副教授

Advisor: Feng-Chiao Tsai, MD Ph.D.

中華民國 112 年 8 月

August, 2023

doi:10.6342/NTU202303790

國立臺灣大學碩士學位論文
口試委員會審定書
MASTER'S THESIS ACCEPTANCE CERTIFICATE
NATIONAL TAIWAN UNIVERSITY

探討 FGFR 介導 TGFβR 訊息如何調控 Fibroblast 分化成 Adipocyte 或 Myofibroblast 的機制

FGFR Mediates TGFβR Signaling to Switch Fibroblast Differentiation between Adipocytes and Myofibroblasts

本論文係_洪堂萌_（R10443004）在國立臺灣大學__藥理學研究所_完成之碩士學位論文，於民國_112 年 6 月 29_日承下列考試委員審查通過及口試及格，特此證明。

The undersigned, appointed by the Department / Institute of _____Pharmacology_____ on 29 / 6 / 2023 have examined a Master's thesis entitled above presented by_Tang-Meng, Hong__ (R10443004) candidate and hereby certify that it is worthy of acceptance.

口試委員 Oral examination committee:

蔡丰喬	鄭乃禎	洪敏杰
（指導教授 Advisor）		
	張玉芳	

系主任/所長 Director:

致謝

時光飛逝，這兩年在台大藥理所的生活緊湊及充實。首先謝謝我的家人，謝謝你們尊重我的選擇進入藥理所就讀。再來，真的十分感謝我的指導教授丰喬老師，尊重我在實驗設計上的規劃，並且樂意與我討論及解決實驗上的問題。此外，蔡老師支持我畢業後出國深造，在繁忙之餘還是會時常和我聊個幾句，並且也對於我未來職涯的規畫給予獨特且務實的建議，像是成為 MD-PhD 的經驗。老師對於我而言就是一個非常值得敬佩的 physician scientist 榜樣。另外也要感謝我的口試委員張玉芳老師、涂熊林老師以及鄭乃禎老師，在我的 committee 以及 defense 除了給予許多實驗上的建議外，也提出我和蔡老師都沒有設想到的問題，這些寶貴的指引對我的計畫幫助巨大，並且讓我夠更像學者一樣的思考問題。

在這棟整體氣氛沉重、步調快速的台大醫學院中，我在 FCTlab 的生活除了工作外也有許多趣事，在繁忙的實驗中和我的好夥伴們保持歡樂的心情。蘭達是一個步調快速且效率高的歡樂女強人，而 Coco 則是詼諧且務實的人生導師，雖然妳們常常和其他人笑我長得像短尾袋鼠，但也感謝你們願意與我討論實驗規畫(當然我也常當你們的 puromycin 小天使啦)。也謝謝庭瑋，幸好有你這個可靠的學妹監督笨笨的我，我們的 project 中成功做出了好多質體和抽了好多菌。感謝朱怡，我的大姐兼聯合其他人欺負袋鼠堂萌的主謀，除了教我染 fiber 的實驗外也常常跟我討論，餵我好多點心跟吃的。謝謝鈺喬，實驗室的老大，謝謝妳帶我們這些屁孩們出去玩和吃東西，去美國開會時帶領我和 coco 兩個鄉巴佬東走西走。謝謝耀斌，雖然你都不把我當學長，和其他人尤其是朱怡一直欺負我、戳我，但你真的幫了我許多忙，你學習實驗認真的態度也值得敬佩。也謝謝冠志，欺負我的同時也給我許多做事及社交上的建議和技巧，祝福你遇到很多帥哥。謝謝軒兆，你教我非常多實驗的技巧跟守則，我覺得我實驗上有許多的操作紅利都是因為有你的毫不吝嗇的指教。謝謝沛儒，在我快畢業的那個時候正因為硬碟爆掉而崩潰之時，成為我的救命稻草協助我 data 上的備份。謝謝琪琳，剛來實驗室的時侯妳教我很多基礎的實驗操作，而且也充當我們這群屁孩的幼兒園園長，祝福妳在美國能夠事事順利。也謝謝新加入的立昂，你講話幽默外也非常認真，簡直就是另一個不會欺負我的耀斌。碩士班的生活結束了，謝謝你們成就了我這兩年辛苦但卻精采無比的人生經歷。

doi:10.6342/NTU202303790

摘要

甲狀腺眼病 (Thyroid eye disease, TED) 是一種常見於葛瑞夫茲氏症 (Graves' disease) 病患上的嚴重眼組織病變。在 TED 患者的眼眶中充滿脂肪及纖維化組織的現象與細胞生長激素訊號的異常活動有關。纖維母細胞生長因子 (Fibroblast growth factors, FGFs) 是一種對纖維母細胞增生和分化成脂肪細胞中扮演關鍵角色的生長因子。我們近期的研究發現，TED 患者血清中 FGF 的水平有上升的現象，且利用 FGF1 刺激自眼窩中分離的纖維母細胞能夠將其轉化為前脂肪細胞 (pre-adipocytes)；利用 FGFR 磷酸酶抑制劑則是其轉化為肌纖維母細胞 (myofibroblasts)。

由於 FGFR 訊息傳遞能夠藉由 micro RNA let-7 和 miR-20a 調控轉化生長因子 β (TGFβR) 訊息，我們檢測了 FGF 是否能通過改變 TGFβR 訊號影響 HS68 纖維母細胞的分化。利用免疫墨點法，我們確認了 TGF-β 能夠增加細胞纖維化指標 α 平滑肌肌動蛋白 (α-smooth muscle actin, α-SMA) 的蛋白表現量，而同時加入 FGFR 磷酸酶抑制劑能夠增強這種效應，這與我們先前在眼窩纖維母細胞所觀察到的纖維化影響相符。另外在免疫螢光染色的結果也發現，抑制 FGFR 激酶活性極大的增強了 TGF-β 誘導的 α-SMA 應力纖維和 F-actin 細胞骨架的重塑，更加說明了 FGFR 在 TGFβR 訊號中扮演著關鍵角色。此外，利用慢病毒剃除 FGFR1 更近一步的加強了 TGFβ 誘導的應力纖維形成的同時卻抑制了整體細胞骨架重塑的活性。令人訝異的是，我們於免疫墨點法的結果發現到 FGFR 的剃除明顯地減弱了 TGFβ 造成的 α-SMA 蛋白表現的增加，與先前免疫螢光染色的發現不一致。這種細胞結構上與蛋白表現量的差異暗示著 FGFR 訊息對 TGFβR 誘導 HS68 纖維母細胞的分化中有著複雜的調控關係。

此研究藉由細胞模型研究 TED 背後的致病機制，並希望最終能夠為該疾病開發基於 FGFR-TGFβR 訊息調控關係的治療方法。

關鍵字：甲狀腺眼病、纖維母細胞生長因子受體、轉化生長因子 β 受體、纖維母細胞分化、纖維化、應力纖維、肌動蛋白細胞骨架

doi:10.6342/NTU202303790

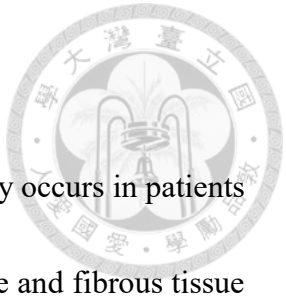

Abstract

Thyroid eye disease (TED) is a severe orbitopathy that frequently occurs in patients of Grave's disease. TED patients suffer from accumulation of adipose and fibrous tissue within the orbital cavity, indicating aberrant activities of growth hormone signaling. Fibroblast growth factors (FGFs) is a growth hormone that playing a crucial role in regulating fibroblast proliferation and differentiation into adipocytes. Our recent work revealed that serum levels of FGFs were elevated in patients of TED, and that FGF1 transformed orbital fibroblasts into pre-adipocytes while FGFR inhibitors transformed them into myofibroblasts.

Since FGFR signaling regulates TGFβR signaling through microRNAs let-7 and miR-20a, we examined if FGF effects on HS68 fibroblasts were also through TGFβR modulation. Using immunoblots, we confirmed that TGF-β increased the expression of alpha smooth muscle actin (α-SMA) protein, the marker of fibrosis, and that FGFR inhibitors enhanced this effect, compatible with our previous results of FGF effects on orbital fibroblasts. Immunofluorescence also indicated that inhibition of FGFR kinase activity greatly increased TGF-β-induced α-SMA stress fiber formation and F-actin cytoskeleton remodeling, supporting the pivotal role of FGFR on TGFβR signaling. Knockdown of FGFR1 further expedited TGF-β-induced stress fiber while repressed

doi:10.6342/NTU202303790

overall actin intensity. Surprisingly, immunoblots indicated that knockdown of FGFR reduced TGF-β effects on α-SMA protein expression, deviating from our immunofluorescence findings. The discrepancy implied the complex nature of FGFR signaling on TGFβR modulation on HS68 fibroblast differentiation.

This project is to elucidate the mechanisms behind TED, with the ultimate goal to develop valid FGFR-TGFβR-based therapy for the disease.

Key words: TED, FGFR, TGFβR, fibroblast differentiation, fibrosis, stress fiber, actin cytoskeleton.

doi:10.6342/NTU202303790

Table of content

doi:10.6342/NTU202303790

doi:10.6342/NTU202303790

doi:10.6342/NTU202303790

Figures and Legends

doi:10.6342/NTU202303790

doi:10.6342/NTU202303790

Tables

doi:10.6342/NTU202303790

List of Abbreviations

TED	Thyroid eye disease
FGFRs	Fibroblast growth factor receptors
TGF-β	Transforming growth factor Beta
α-SMA	Alpha-smooth muscle actin
GD	Grave's disease
TSAbs	Thyroid-stimulating autoantibodies
TSHR	Thyrotropin receptor
RTKs	Receptor tyrosine kinases
VEGFRs	Vascular endothelial growth factor receptors
ECM	Extracellular matrix
SMAD3	SMAD family member 3
DAPI	4′,6-diamidino-2-phenylindole
SDS-PAGE	SDS-polyacrylamide gel electrophoresis

doi:10.6342/NTU202303790

Chapter 1 Introduction

1.1 Overview of Thyroid eye disease

Grave's disease (GD) is a severe autoimmune disease affecting thyroid gland's functionalities. This disorder is characterized by overproducing thyroid-stimulating autoantibodies (TSAbs) that activates the thyrotropin receptor (TSHR) and result in hyperthyroidism and extrathyroidal inflammation of other organs. [1, 2] Still, the general mechanism of how autoantibodies are produced in the body is still unclear. Several manifestations such as thyrotoxicosis, dermopathy, goiter and orbitopathy were commonly found in Grave's disease patients. [1, 3] Graves' ophthalmopathy, also known as thyroid eye disease (TED), are frequently present in GD patients. About 40% ~ 50% of GD patients will develop TED in their onset. [4-6] Prevailing traits of TED are proptosis, congestion, eyelid retraction, and optic neuropathy which greatly affecting may patients' quality of life and social confidence. [4, 7-9]

Treatments of TED are dependent on how severity of disease is presented by the patient. [9] From mild to moderate symptoms, lubricating eye drops, lifestyle adjustments such as limit sodium intake and elevated sleeping posture, anti-inflammatory agent corticosteroids are considered to used. [9-11] Currently, severe TED symptoms that are

doi:10.6342/NTU202303790

vision-threatening could only be solved effectively by surgical intervention and radiotherapy. [11, 12] Clinical findings suggested that pathogenesis of TED involves of adipogenesis and fibrosis from abnormal orbital fibroblast activities. [13, 14] However, how these pathological process happens is still need to be elucidate.

1.2 Growth factors signaling and TED

Receptor Tyrosine Kinases (RTKs) are responsible for several cellular purposes, including proliferation, differentiation, metabolism, and cell survival. Several studies indicated that irregulated of RTK signaling is associated with disease such as cancer and embryonic defects. [15, 16] Clinical studies also reported that increased blood vessel density was found during acute TED inflammation. In addition, the expression level of vascular endothelial growth factor receptor (VEGFR) and VEGF signaling ligands were all elevated in TED orbital tissue. [17] Another research also found that small-molecule VEGFR inhibitor Lenvatinib have prominent therapeutic effect on TED, by suppressed orbital angiogenesis and adipogenesis. [18] Moreover, clinical trial of anti-VEGF therapy for acute TED is in progress. Together, these findings imply that abnormal angiogenesis occurs in TED pathogenesis.

doi:10.6342/NTU202303790

Besides VEGFR, another RTK Fibroblast growth factor receptor (FGFR) is also considered as an inducer for angiogenesis and adipogenesis among several tissues. The therapeutic effect of VEGFR inhibitor on TED observed in the study is likely due to inhibition of angiogenesis induced by both VEGFR and FGFR. Nevertheless, orbital fibroblast is the prominent driver for TED fibrosis and inflammation. FGFR, as its names implies, plays crucial role in regulating fibroblast proliferation and differentiation to become adipocytes. [19] We then assumed the possibility that FGFR signaling also have a large impact on TED pathogenesis.

1.3 TGF-β signaling induces fibrosis in TED

Fibrosis is regarded as a pathological wound healing response to persistent injury or inflammation that affects nearly every tissue such as liver, kidney or lung in the body. [20] This pathological feature is defined as the extensive deposition of extracellular matrix (ECM). Studies and reports of pathology from different organs have revealed that fibrosis happened at different tissue may all share some sort of similarity in the profibrotic signaling to drive the process, suggesting that distinct causes of tissue injury may all result in activation of a common fibrogenic pathway that trigger the develop of chronic fibrosis. [20,21]

doi:10.6342/NTU202303790

One representative phenotype of TED is severe fibrosis around orbital tissue. The main contributor of fibrosis in this disease is orbital fibroblast. The activation of orbital fibroblast results in the differentiation into myofibroblast. [22, 23] Myofibroblast serves as a key role of producing excessive deposition and regulating remodeling of ECM complex proteins. [20, 21] These cellular responses will ultimately cause fibrosis formation. Among several profibrotic signaling, TGF-β signaling is considered to be the strongest driver for fibrosis. This signaling is a key regulator for tissue development, wound healing and activation of fibroblasts. However, prolonged inflammation-induced high level of TGFβR signaling may lead to irreversible fibrogenesis. [24, 25] In severe TED, abnormal fibrosis is observed and possibly due to potent orbital tissue remodeling caused by inflammatory microenvironment and other related cytokines. Furthermore, several studies have reported that dysregulated TGF-β signal and its receptor expression exists in orbital tissue of TED patients. These data all suggested that TED-derived fibrosis is highly related to myofibroblast differentiation induced by TGFβR signaling.

However, the molecular mechanism of TED developed TGFβR signaling related fibrosis, the preference of forming either fibrosis or adipogenesis or both and how this pathological progression is still not clear. Interestingly, previous study suggested that FGFR may regulate TGFβR signaling through microRNAs let-7 and miR-20a. [26] In

doi:10.6342/NTU202303790

other words, the production of these miR induced by FGFR signaling may reduce expression level of TGFβR receptor and attenuate latter's functionality.

Thus, we started to investigate the role of fibroblast at the diseases and the regulation of TGFβR and FGFR signaling on its functionalities in vitro.

1.4 FGFR regulated TGF-β signaling in complex manners in cell model

Our recent work found that serum levels of FGF1 and FGF2 were elevated in TED patients. Also, we observed that FGF1 transformed orbital fibroblasts form TED patients into pre-adipocytes while FGFR inhibitors tended to transformed them into myofibroblasts (**Figure 1**) We then performed immunoblotting to assay HS68 fibroblast cells and the data indicating that FGFR agonist FGF1 suppressed TGF-β-induced fibrotic marker alpha-smooth muscle actin (α-SMA) expression, while FGFR kinase inhibitor AZD4547 could not only reverse this effect also strengthen the amount of α-SMA detected by the assay (**Figure 2A**). The phosphorylated SMAD3, the activation sign of TGFβR signaling, also reduced by FGF1 but enhanced by AZD4547 with a similar pattern of what α-SMA exhibited. Moreover, the elevated levels of α-SMA and p-SMAD3 expressions caused by AZD4547 could further be attenuated by direct TGFβR inhibitor SB525334 and SMAD3 inhibitor SIS3.

doi:10.6342/NTU202303790

To our surprise, we observed that knock down of FGFRs on HS68 cells decreased TGF-β-induced α-SMA expression (Figure 2B) but not affect phosphorylation of SMAD3 (Figure 3A). Overexpression of FGFR1 only increased α-SMA level when AZD4547 existed. Together, these findings suggested that FGFR suppressed TGFβR signaling via its kinase activity, but it also promoted TGFβR signaling in alternative kinase-independent manner.

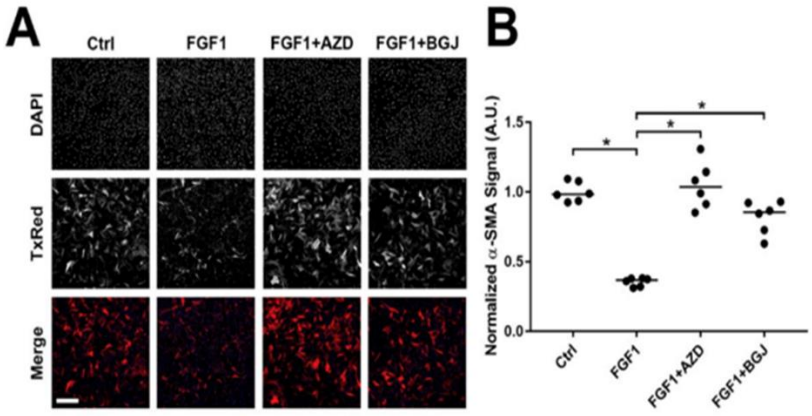

Figure 1 FGFR inhibitors induced the differentiation of orbital fibroblasts from TED patients into myofibroblasts.

(A) Representative immunofluorescence images of α-SMA staining showed that FGF1 suppressed fibroblast differentiation into myofibroblasts and this effect was reversed by FGFR inhibitors. (B) Dot plot of quantified α-SMA signal.

doi:10.6342/NTU202303790

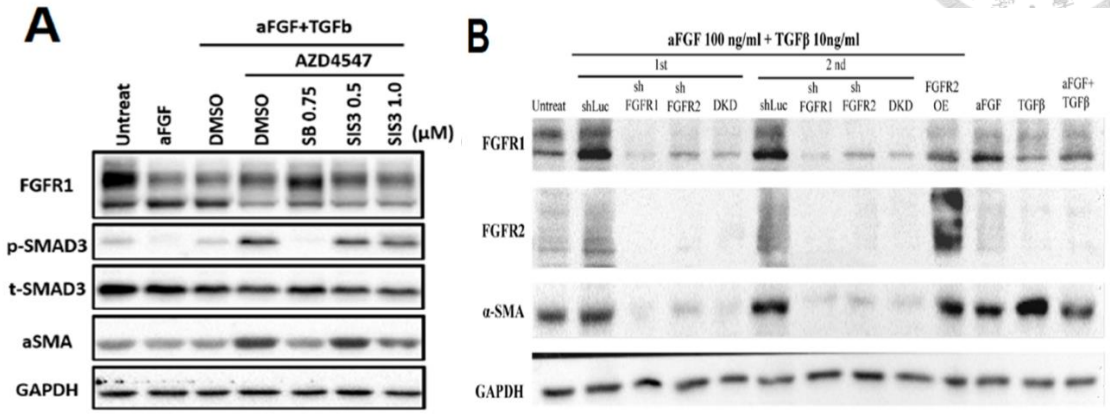

Figure 2 FGFR regulated TGFβR signaling via both kinase-dependent and kinase-independent manners

(A) Immunoblotting indicated that FGFR kinase inhibitor AZD4547 increased TGF-β-induced α-SMA and p-SMAD3 protein level, and this phenomenon was attenuated by TGFβR inhibitor SB525334 and SMAD3 inhibitor SIS3.

(B) Knockdown of FGFR1 surprisingly decreased α-SMA protein level.

doi:10.6342/NTU202303790

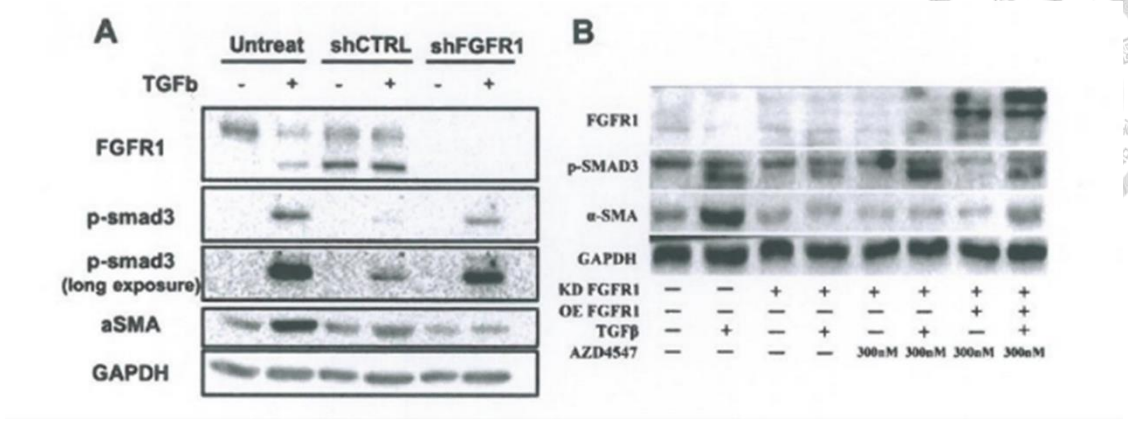

Figure 3 Knockdown and Overexpression of FGFR1 receptor did not affect the phosphorylation of SMAD3

(A) The immunoblotting indicated that knockdown of FGFR1 did not affect the phosphorylation of SMAD3, the downstream target of TGFβR, when α-SMA reduced.

(B) SMAD3 activation also did not influenced by overexpression of FGFR1 and only AZD4547 could enhance α-SMA level.

1.5 The specific aim

In this project discussing molecular mechanisms behind TED, we sought to investigate the role of FGFR in TGFβR signaling and clarify how FGFR "switch" TGFβR-related downstream pathways in HS68 fibroblast model.

doi:10.6342/NTU202303790

Chapter 2 Material and Methods

2-1 Cell culture

HS68 cells were purchased from Bioresource Collection and Research Center (BCRC), The food industry research and development institute (FIRDI), Taiwan. Cells were maintained and at 37°C and 5% CO_2. The cells were delicately grown in Dulbecco's modified Eagle's medium (DMEM; Gibco, Thermo Fisher Scientific, Waltham, MA, USA and HyClone, Logan, UT, USA). Culture medium for HS68 cells was supplemented with 1% of penicillin/streptomycin (P/S) (Gibco) and 10% fetal bovine serum (FBS; HyClone). Fresh medium was replaced every 2 to 3 days. The cells were passaged using 0.5% trypsin EDTA solution (Gibco)and rinsed with phosphate-buffered saline (PBS) (Corning, New York, USA), within no more than 10 passages after initial thawing.

2-2 Construction of Overexpression FGFR1 KD plasmids

Previous studies reported that the residues D623 and Y653/Y654 of FGFR1 are important to its kinase functionality [27,28]. The mutations D623A and Y653F/Y654F would greatly hamper its kinase activities and receptor autophosphorylation process.

doi:10.6342/NTU202303790

Thus, we decided to generate FGR1 plasmids containing these 2 mutations for our study. Plasmid pLAS2W-FGFR1-P2A-EYFP was generated by lab senior. To generate plasmid containing FGFR1 that lack of kinase activities, site directed mutagenesis were performed. First, primer pairs were designed on takara.teselagen.com. The pLAS2W-FGFR1-P2A-EYFP was performed PCR reactions, either flanked by primers FGFR1 D623A.For and FGFR1 D623A.Rev or primers FGFR1 Y653/654F.For and FGFR1 Y653/654F.Rev, respectively. To eliminate DNA template, PCR products were mixed with DPN I enzyme (New England Biolabs) and incubated in 37°C for 2 hours for fully digestion. The DNA products were performed electrophoresis on agarose gel. Region included products of interest were isolated and purified by NucleoSpin Gel and PCR Clean-up kit (MACHEREY-NAGEL). 100 ng of filtered DNA was ligated by In-Fusion® HD Cloning Kit (Takara) and transformed into Stbl3 competent cell. Single colony containing pLAS2W-FGFR1(D623A)-P2A-EYFP and pLAS2W-FGFR1(Y653/654F)-P2A-EYFP were selected and performed Miniprep and Midiprep were used to amplify plasmids. All DNA sequences were verified by Genomics BioSci & Tech Co., Ltd.

doi:10.6342/NTU202303790

2-3 Lentivirus package

Clones of Lentivrus use for FGFR1 knock down were purchased from RNAi core. HEK293T cells was passaged on 10 cm culture dishes overnight and transfected with liposome-based mixture of 6.75 μg of shRNA, 7.5 μg of pCMVDR8.91 and 750μg of pMD2G plasmids for 24 hours. Medium was replaced with fresh DMEM medium containing 1% Bovine serum albumin (BSA). The medium was harvested and filtered through 0.45μm PES filters and mixed with Lenti-X Concentrator (Takara) overnight. The mixture was pre-cooling and centrifuged at 1500 g for 50 mins and the supernatant was discarded. Viral pallet was resuspended by regular DMEM containing 10% FBS.

2-4 Cell Counting Kit-8 (CCK-8) assay

HS68 fibroblast cells were seeded at rat collagen coated-96 well (Corning) at the density of 3000 per well overnight and infected with different amounts of viruses (from 0.5 to 2μl) for 24 hours flowing by certain antibiotics selection (puromycin or blasticidin). Medium was replaced by 100 μl of DMEM containing CCK8 solution and incubated for 1 hour and Absorbance 450 nm (OD 450) was measured by microplate spectrophotometer.

doi:10.6342/NTU202303790

The values of OD 450 were then calculated and convert into the multiplicity of infection (MOI) to determine amount of virus used for infection in each experiment.

2-5 Immunofluorescence staining of stress fiber

To induce myofibroblast differentiation, HS68 fibroblasts (3000 cells/well) were seeded on rat collagen-coated (3 μg/μl) 96-well. Surrounding wells were placed with double distilled water (ddH_2O) to keep the moisture. After overnight attachment, the original medium was changed to DMEM containing 0.1% FBS. TGF-β (10 ng/ml; PeproTech, Rocky Hill, NJ, USA), FGF1 (100 ng/mL) or the combination of FGF1 and FGFR kinase inhibitor AZD4547 and BGJ398 (100 mM) were added in each test groups. Before fixation, HS68 cells were incubated for 48 to 96 hours depends on the purposes.

To detect myofibroblast marker α-SMA, cells were first rinsed by 100 μl of cold PBS once and then fixed with mixture of acetone/methanol (1:1) solution at −20°C for 5 min. The fixed HS68 cells were carefully rinsed by cold PBS 3 times, each time for 5 mins, to keep cell from detachment from the 96 wells and blocked in 50 μl Tris Buffered Saline with Tween-20 (TBST) with 5% BSA on shaker about 1 hour to prevent nonspecific binding of other proteins against the following primary antibody.

doi:10.6342/NTU202303790

Next, cells were incubated in 50 μl TBST with 5% BSA containing α-SMA antibody (Anti α-SMA anti-rabbit antibody, Abcam, catalog no. ab5694, 1:100 dilution) at 4°C overnight and then incubated with 50 μl Alexa Fluor 594 dye–conjugated secondary antibody (1:500) and 10 μg/ml of DAPI (or 1 μg/ml of Hoechst 33342) in TBST solution with 5% BSA for 1 hour. A fluorescence microscope (Nikon DS-Qi2) was used to detect fluorescence of α-SMA (594 nm) and nuclei, respectively. The signal of α SMA and nuclei would further be quantified by MATLAB code to define intensity of stress fiber structure. Details of the procedure were depicted in Figure 1.

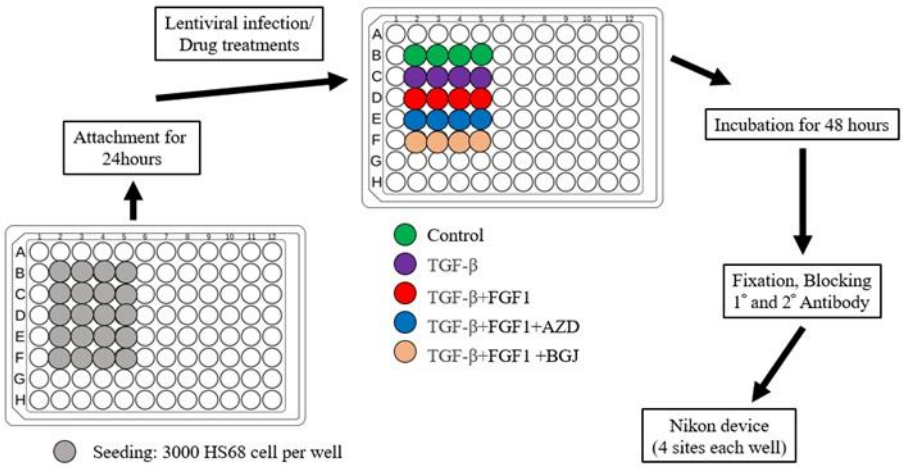

Figure 4 Procedure of α-SMA immunofluorescence staining

doi:10.6342/NTU202303790

2-6 Immunofluorescence staining of actin cytoskeleton

To detect cytoskeleton remodeling, HS68 cells treated with drugs (described above) were first gently rinsed with 100 μl of cold PBS once and fixed with 50 μl of 4% paraformaldehyde (Sigma) in PBS solution for 10 mins, following by 10 mins of permeabilization with 50 μl of 0.25% Triton X-100 solution (J.T.Baker®, Phillipsburg, NJ, USA) at room temperature. The permeabilized HS68 cells were blocked with 50 μl TBST containing 5% BSA for an hour. Cells were then incubated with 50 μl TBST with 5% BSA containing Alexa Fluor™ 594 Phalloidin (Thermo Fisher Scientific) and 1 μg/ml of Hoechst 33342 (Thermo Fisher Scientific) for 1 hour at room temperature on shaker. After rinsed with PBS 3 times, the fluorescence microscope (Nikon DS-Qi2) was used to detect actin filaments. Quantification of actin signal was based on MATLAB code.

doi:10.6342/NTU202303790

2-7 Western blot

2-7-1 Protein extraction

HS68 cells were plated at 6 cm dishes at the density of 300000 cells per dish overnight and infected with viruses or treated with TGF-β (10 ng/ml; PeproTech, Rocky Hill, NJ, USA), FGF1 (100 ng/mL) or a combination of FGF1 and FGFR kinase inhibitors (100 mM) or both. Cells were fully lysed by radioimmunoprecipitation assay lysis buffer (Cell Signaling Technology, Danvers, MA, USA) supplemented with protease and phosphatase inhibitor cocktail (PPIC, Thermo Fisher Scientific). Lysates were collected and incubated on ice for 30 mins and then centrifuged for 10 mins at 15,000 rpm to remove cell debris. The amount of protein was quantified by Pierce™ BCA Protein Assay Kit (Thermo Fisher Scientific). Total 15 ug of protein from lysates was mixed with 5x protein loading dye containing β- Mercaptoethanol (Beta-ME) and heated in 95°C for 10 mins to denature protein samples. Denatured protein was stored at -20°C for further usage.

doi:10.6342/NTU202303790

2-7-2 Gel-based electrophoresis and protein transfer

SDS-PAGE gel was constructed by Biorad system. Briefly, protein samples and marker were loaded into wells of SDS-PAGE. Electrophoresis was set to performed at 75 V constant voltage for 30 mins following by 110 V constant voltage for additional 90 mins. Then protein was transferred from gel to nitrocellulose membranes at 110 V constant voltage for 120 mins on ice.

2-7-3 Primary and secondary antibody conjugation

The membranes were cut based on sizes of interested proteins and blocking at TBST+5%BSA solution for 1 hour. The membranes were replaced into TBST+5%BSA solution containing corresponding primary antibodies and shacked overnight. The membranes were gently rinsed by pure TBST solution3 times, 3 mins each time. After the wash step, the membranes were placed into TBST+5%BSA containing secondary antibodies for 1 hours on the shaker.

doi:10.6342/NTU202303790

Primary antibody			
Target protein	**Brand**	**Dilution ratio**	**source**
FGFR1	Cell Signaling® #9740	1:2000	rabbit
GAPDH	Invitrogen®, #AP7873b	1:5000	mouse
GAPDH	ABGENT®, #AP7873b	1:5000	rabbit
TGFβR1	Abcam®, #ab121024	1:2000	rabbit
α-SMA	Abcam®, #ab5694	1:2000	rabbit
Secondary antibody			
Anti-rabbit IgG-HRP	ABGENT® LP1001c	1:5000	Goat
Anti-mouse IgG-HRP	ABGENT® LP1002c	1:5000	Goat

Table 1 Antibodies used for western blot

2-7-4 Chemiluminescent immunoassay and quantification

Membranes conjugated with secondary antibodies were washed 3 times, each time for 5 mins, and soaked into the mixture of enhanced chemiluminescent substrates (ECL, T-Pro Biotechnology, New Taipei City, Taiwan). The signal from excited substrates was then detected by ChemiDoc™ MP Imaging System (Bio-Rad). The following quantification of signal intensity was performed by ImageJ Fiji.

doi:10.6342/NTU202303790

Chapter 3 Results

3.1 FGFR signaling alters TGF-β events in HS68 fibroblast

3.1.1 TGF-β-induced stress fiber formation was attenuated by ligand-induced FGFR activation

First, we tested the effect of manipulating FGFR signaling on TGF-β-induced event on HS68 cell model. Based on previous data, we knew that the dominant FGFR isoform expressed on HS68 is FGFR1. Two FGFR kinase inhibitors AZD4547 and BGJ398 were used to created kinase blockade, and FGFR1 agonist FGF1 (acidic-FGF) was used as an activator of FGFR signaling. On the other hands, TGF-β1 was used to drive fibrosis event via its counterpart receptor TGFβR and downstream activation. We performed immunofluorescence of α-SMA, an indicator commonly used to evaluate myofibroblast activation and fibrotic transition, to see how FGFR signaling acts on TGF-β-induced fibrotic event. We observed that administration of TGF-β could partially induce α-SMA -based stress-fiber structure and co-treatment of FGF1 would repress fiber formation. (Figure 5A) This effect was corresponding with the previous finding that FGF1 could induce adipogenesis on fibroblasts away from myofibroblast-like phenotypes. In addition,

doi:10.6342/NTU202303790

co-treatment of TGF-β, FGF1 with FGFR kinase inhibitors AZD4547 or BGJ398 not only attenuate inhibition of fibrosis caused by FGF1, but significantly induce potent stress fiber formation compared to treat TGF-β alone, indicating that formation of stress fiber induced by TGF-β stimulus was repressed by FGFR signaling via its kinase activity.

Also, immunoblotting was used to detect the global protein level changes upon receptors activation. Similarly, we observed that the α-SMA protein level was elevated in cells stimulated with TGF-β, with FGFR kinase inhibitor AZD4547 markedly increased TGF-β-induced α-SMA expression (Figure 5B and 5C). When FGF1 existed, α-SMA protein level induced by TGF-β was decreased compared to control DMSO-treated group. Intriguingly, FGF1 alone did not repress α-SMA level, which is distinct from cells stimulated with FGF1 and TGF-β simultaneously.

doi:10.6342/NTU202303790

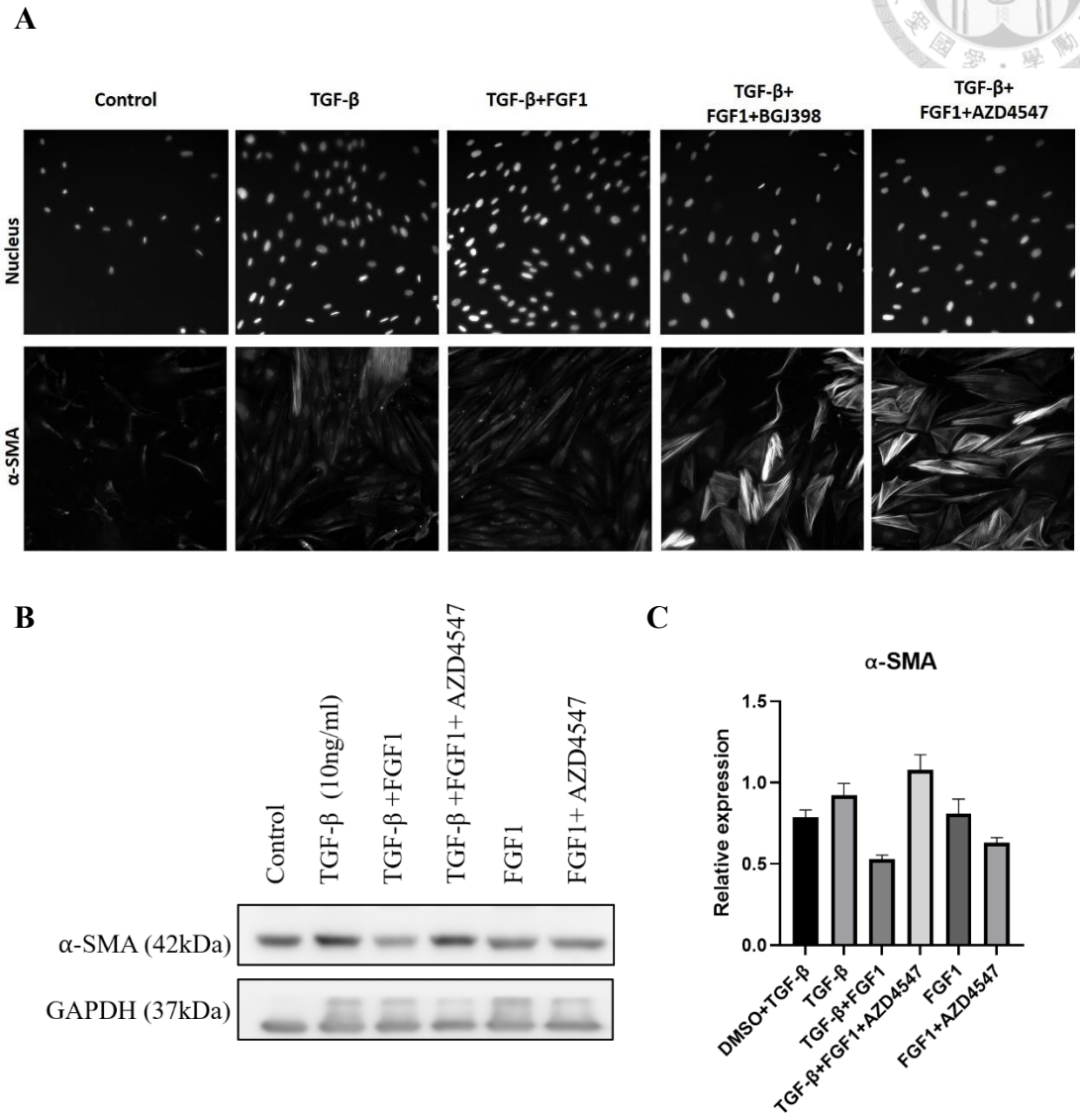

Figure 5 FGFR signaling repressed stress fiber formation in HS68 fibroblasts

(A) Hs68 fibroblasts were incubated with TGF-β with or without FGF1, FGFR inhibitors AZD4574 or BGJ398 for 48 hours. Cells were then fixed with 1:1 Acetone / methanol. Fibrotic marker α-SMA signal was examined by immunofluorescence. Nuclei were stained by DAPI simultaneously.

doi:10.6342/NTU202303790

(B) Hs68 fibroblasts were treated with TGF-β with or without FGF1, FGFR inhibitors AZD4574 or BGJ398 for 48 hours. Total protein was extracted from cells and then analyzed by immunoblotting. The housekeeping gene GAPDH was selected as an independent internal control for global protein expression in this study.

(C) Quantification of western blot was based on the relative level of α-SMA to GAPDH.

doi:10.6342/NTU202303790

3-1-2 Inhibition of FGFR kinase activity could further enhance TGF-β-induced stress fiber formation

Since we observed that FGFR kinase could reverse the inhibition of TGF-β-prompted stress fiber formation caused by FGF1 stimulus, we wondered whether FGFR kinase inhibitors alone could induce α-SMA stress fiber formation even when TGF-β was absent in microenvironment. To exactly exclude this possibility, we then examined the HS68 fibroblast differentiation under TGF-β induction at three distinct backgrounds, achieving by adding DMSO, AZD4547 or BGJ398 into growth medium, respectively.

Comparably, stress fiber formed slightly in the cells incubated with TGF-β at DMSO background. While in the cells incubating at FGFR kinase inhibitor background, TGF-β elicited robust stress fiber formation and myofibroblast-like morphological change on HS68. (Figure 6A) Interestingly, FGFR kinase inhibitor alone could not induce any apparent fiber structure, which repudiates the possibility that has already mentioned above. Besides, immunoblotting based on same design gave similar results. Cells from AZD4547 and BGJ398 background displayed slightly reduced of α-SMA protein level compared to the DMSO background group. Cells treated with TGF-β and DMSO background exhibited marginally increased α-SMA, while potent intensity of the protein

doi:10.6342/NTU202303790

band was observed form cells incubated with TGF-β and FGFR kinase inhibitor background (Figure 6B and 6C).

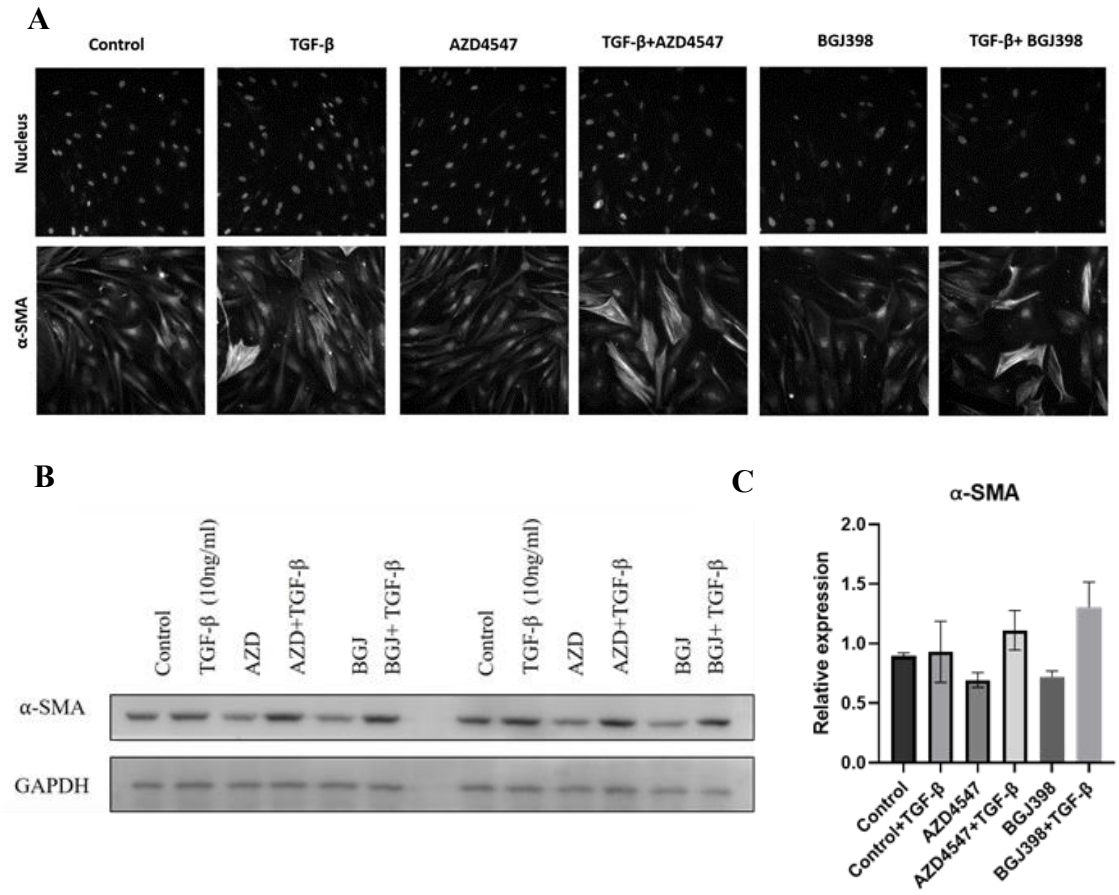

Figure 6 Combination of FGFR kinase blockade and TGF-β could enhance formation of stress fiber and α-SMA protein level

(A) Hs68 fibroblasts were incubated with TGF-β with or without FGFR inhibitors AZD4574 or BGJ398 for 48 hours. Compared to TGF-β alone, co-treatment of TGF-β and FGFR kinase inhibitors significantly increased α-SMA stress fiber formation (B) Hs68 fibroblasts were treated with TGF-β within control DMSO, FGFR inhibitors

doi:10.6342/NTU202303790

AZD4574 or BGJ398 background for 48 hours. Expression levels of protein were examined by immunoblotting. GAPDH was an internal control. (C) Quantification of western blot was based on the relative level of α-SMA to GAPDH.

3-2 FGFR receptor also participated in α-SMA production

3.2.1 Loss of FGFR1 increased stress fiber formation

Since FGFR signaling would attenuate TGF-β-induced stress fiber formation, next we sought to clarify how HS68 fibroblast cells respond to exogenous TGF-β stimulation as FGFR1 receptor is absent. To answer this question, myofibroblast differentiation assay was performed after genetic knock down of FGFR1 receptor by lentiviral infection since FGFR1 is the dominant FGFR isoform in hs68 fibroblast cells.

Cells infected with shFGFR1 showed a noticeable stress fiber formation even when FGFR1 agonist, FGF1, existed in the medium (Fig. 7B). In contrast, cells infected with control lentivirus shLuciferase (shLuc)exhibited a very similar pattern as previous experiments, with cells treated with TGF-β and FGFR kinase inhibitors exhibited most obvious stress fiber formation (Fig. 7A). This finding suggested that loss of FGFR could

doi:10.6342/NTU202303790

enhance stress fiber formation and prevent FGF1-mediated inhibition from its paired ligand-receptor binding.

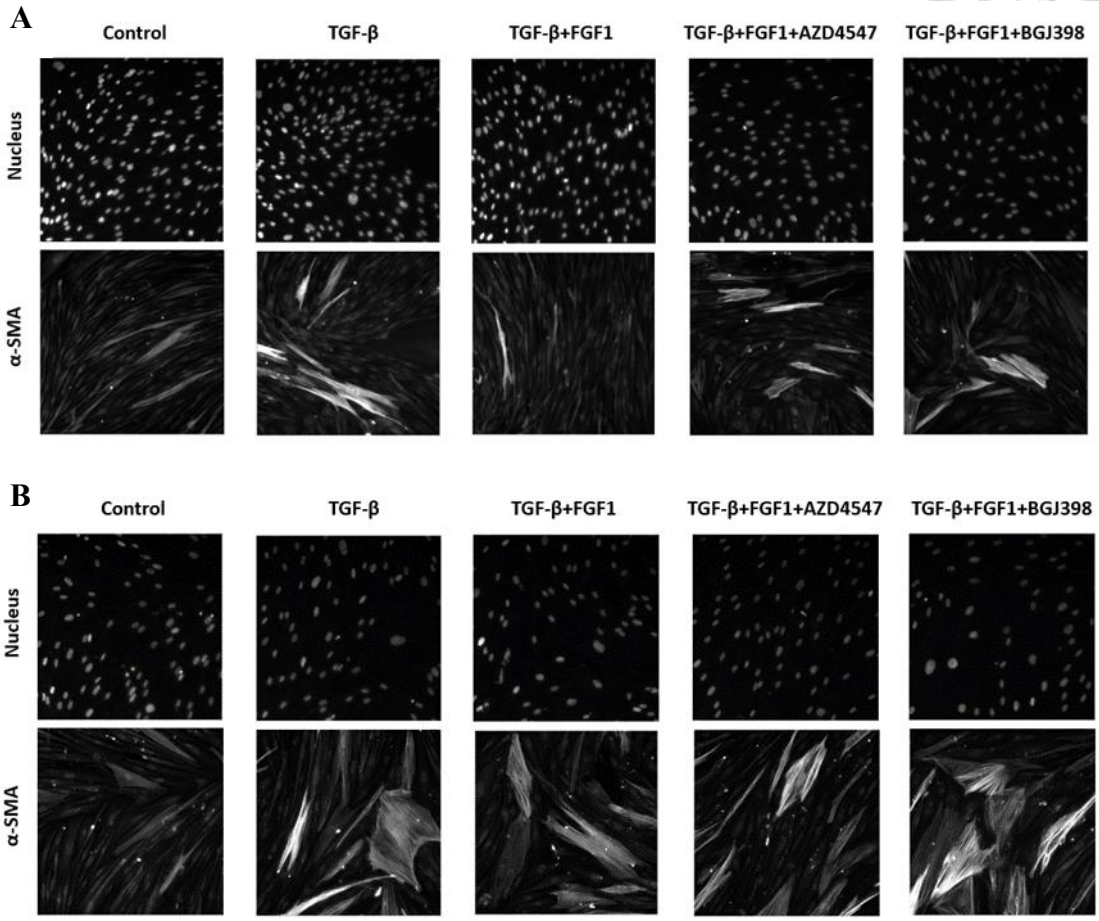

Figure 7 FGFR1 knockdown increased stress fiber formation in HS68 cells

Hs68 fibroblasts were first infected with shLuc (Fig. 7A) or shFGFR1(Fig. 7B) lentivirus for 24 hours. After additional 24 hours of puromycin selection, cells were then incubated with TGF-β with or without FGF1, FGFR inhibitors AZD4574 or BGJ398 for another 48 hours. (A and B) Compared to the control shLuc group, cells infected with shFGFR1 showed a potent stress fiber formation even when FGF1 existed in the medium.

doi:10.6342/NTU202303790

3.2.2 Loss of FGFR1 reduced α-SMA protein expression

Based on previous immunofluorescence findings, we assumed loss of FGFR1 may increase α-SMA protein level. However, immunoblotting data indicated knockdown of FGFR1 decreased α-SMA expression (Figure 8). This phenomenon was distinct from what we observed from immunofluorescence data, suggesting that physical existence of FGFR1 is also important for α-SMA protein expression induced by TGF-β signaling.

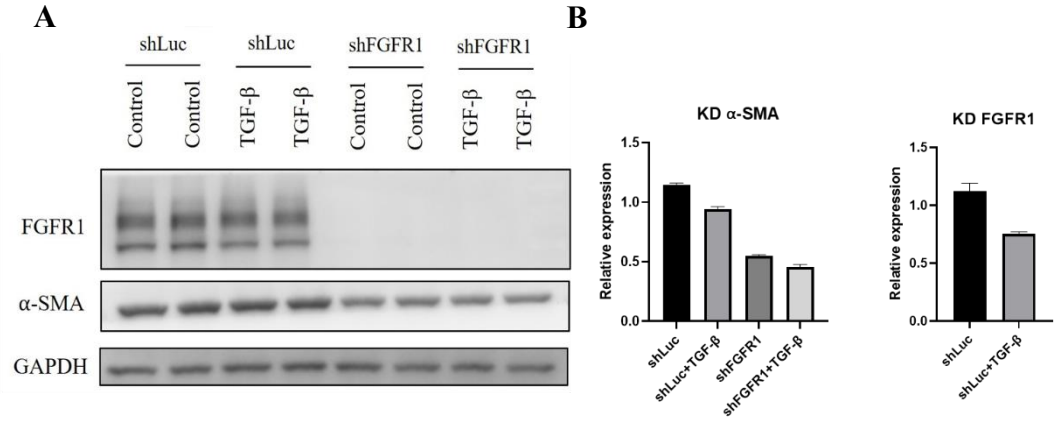

Figure 8 Lentiviral knockdown of FGFR1 reduced α-SMA protein level

(A) Hs68 fibroblasts were infected with control shLuc or shFGFR1 following by puromycin selection and TGF-β treatment for 96 hours. Protein level of α-SMA and FGFR1 were examined by immunoblotting.

(B) Quantified α-SMA and FGFR1 signal were plotted based on the relative level of α-SMA to GAPDH.

doi:10.6342/NTU202303790

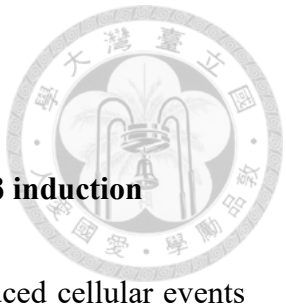

3.2.3 FGFR1 receptor was downregulated against TGF-β induction

Our findings suggested that FGFR1 might mediate TGF-β-induced cellular events in a contextual manner, resulting in discrepancy happened to expression of fiber component α-SMA protein and stress fiber formation.

Thus, the next issue that we were highly interested was whether FGFR1 receptor could be regulated to a certain extent during TGF-β signaling activation. Using immunoblotting we observed compelling difference of FGFR1 receptor expression after TGF-β induction (Figure 9). Cells treated with DMSO plus TGF-β or AZD4547 plus TGF-β both exhibited reduced FGFR1 expression compared to their own background groups. Intriguingly, AZD4547 plus TGF-β group showed a moderately reduced FGFR1 expression compared to AZD4547 group, while DMSO plus TGF-β group had a conspicuous reduction compared to DMSO group. TGF-β-induced FGFR1 reduction could also be observed in FGFR1 knock down experiment, supporting by the evidence that cells infected with control shLuc lentivirus exhibited decreased FGFR1 receptor expression after exogenous supplement of TGF-β (Figure 8A). Together, these immunoblotting results indicated the downregulation of FGFR1 happened after TGF-β induction in HS68 fibroblast cells.

doi:10.6342/NTU202303790

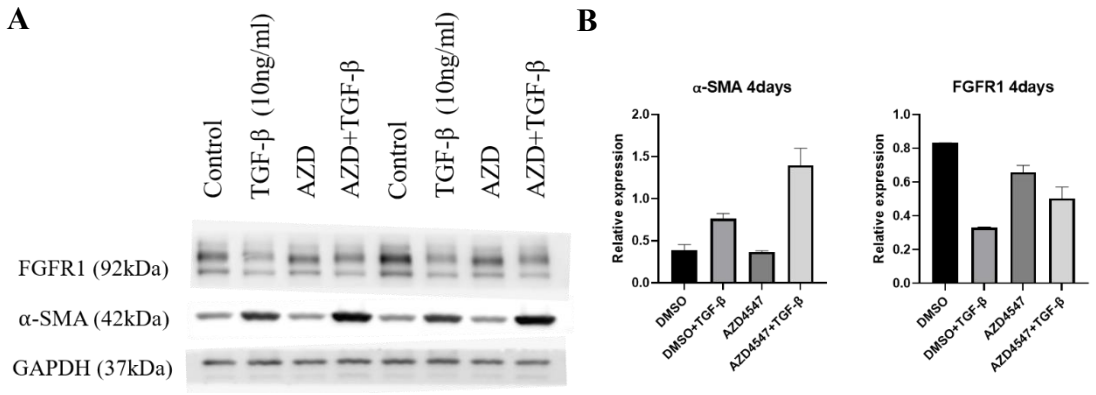

Figure 9 FGFR1 receptor downregulated against TGF-β induction

(A) Hs68 fibroblasts were treated with TGF-β within control DMSO, FGFR inhibitors AZD4574 or BGJ398 background for 96 hours. Protein expression was analyzed by western blot. GAPDH was an internal control.

(B) Quantified α-SMA and FGFR1 signal were plotted based on the relative level of α-SMA to GAPDH.

doi:10.6342/NTU202303790

3-3 The role of FGFR on TGF-β-induced actin cytoskeleton remolding

During myofibroblast differentiation, actin cytoskeleton dynamics plays a crucial role on several cellular events such as focal adhesion and cell contraction [29, 30]. Also, previous studies indicated that cytoskeleton distribution was greatly affected by cell density [31, 32]. To better answer this question, we investigated whether FGFR and TGF-β signaling modulation could have prominent effect on actin dynamics under several cell densities.

Phalloidin was used to labelled F-actin and we observed clear F-actin structure formed in HS68 fibroblast cells. To quantify actin signal correctly, we developed a MATLAB code based on MATLAB software (Figure 10). This code first processed background subtraction to minimize noise on images and created a boundary called “Ring” that surrounding the nucleus based on area where nucleus dye binding. Actin signal inside and outside the ring was calculated into average per pixel and defined as “nucleus signal (N)” and “ring (cytosol) signal (C)”, respectively. Since “C” signal was easily affected by cell shape, crowdedness from neighbor cells and background noisy, “N” signal was selected as a better parameter to represent actin cytoskeleton intensity sue to its relatively accurate circumscription and consistency (Figure 10F).

doi:10.6342/NTU202303790

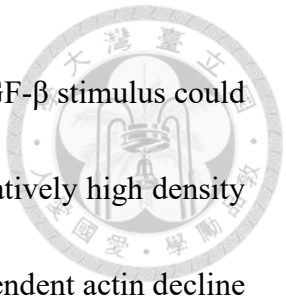

“N” signal was negatively correlated with cell density, while TGF-β stimulus could enhance the actin filaments across the cells even cells plated in a relatively high density and crowed environment (Figure 11A). We assumed this density-dependent actin decline was a direct result of contact inhibition mediated by crowed fibroblasts.

Moreover, combination of TGF-β and FGFR kinase inhibitors AZD4547 and BGJ398 could remarkably induce potent filament pattern (Figure 11A and B). We further plotted histogram to examine whether there has a trend existing on of all cells after TGF-β induction. Histograms of N signal from each groups of cells indicated that cells treated with TGF-β exhibited an integrated and obvious shift to higher degree of intensity, which meaning that TGF-β could trigger most of the cells to expedite enhancement of actin signal rather than subgroup of cells, which is distinct form what we visually observed at α-SMA fiber immunofluorescence data (Figure 11C)

doi:10.6342/NTU202303790

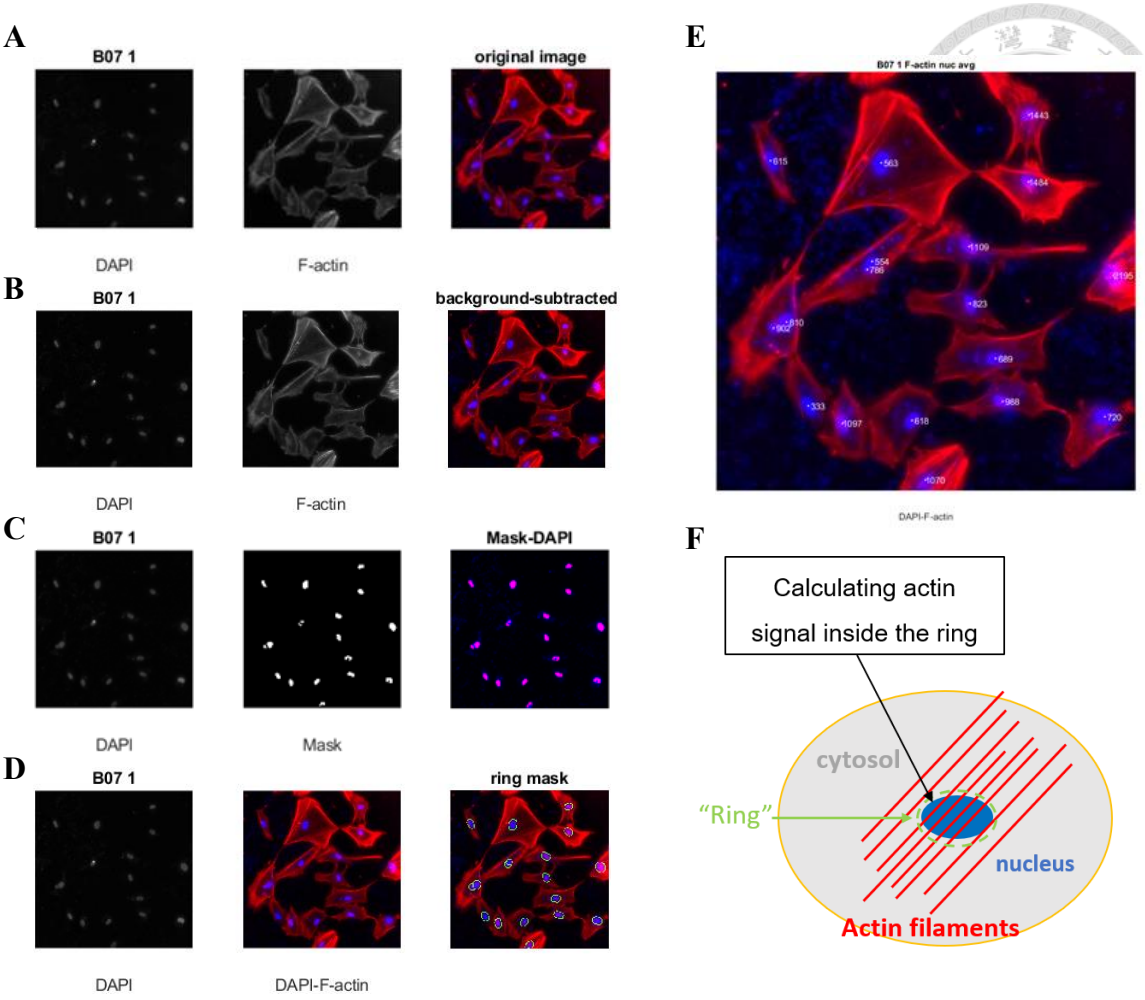

Figure 10 The scheme of quantification of actin signal

The images were first visualized (A) and performed background subtraction (B). Then the nucleus localization was masked based on their nucleus location where DAPI or Hoechst 33342 dye indicated (C). Then the mathematical function "ring" was created to distinguish the phalloidin dye signal on the area of cytosol and nucleus, respectively. (D) We define the phalloidin signal on nucleus (N) as a representation of F-actin cytoskeleton structure. (F)

doi:10.6342/NTU202303790

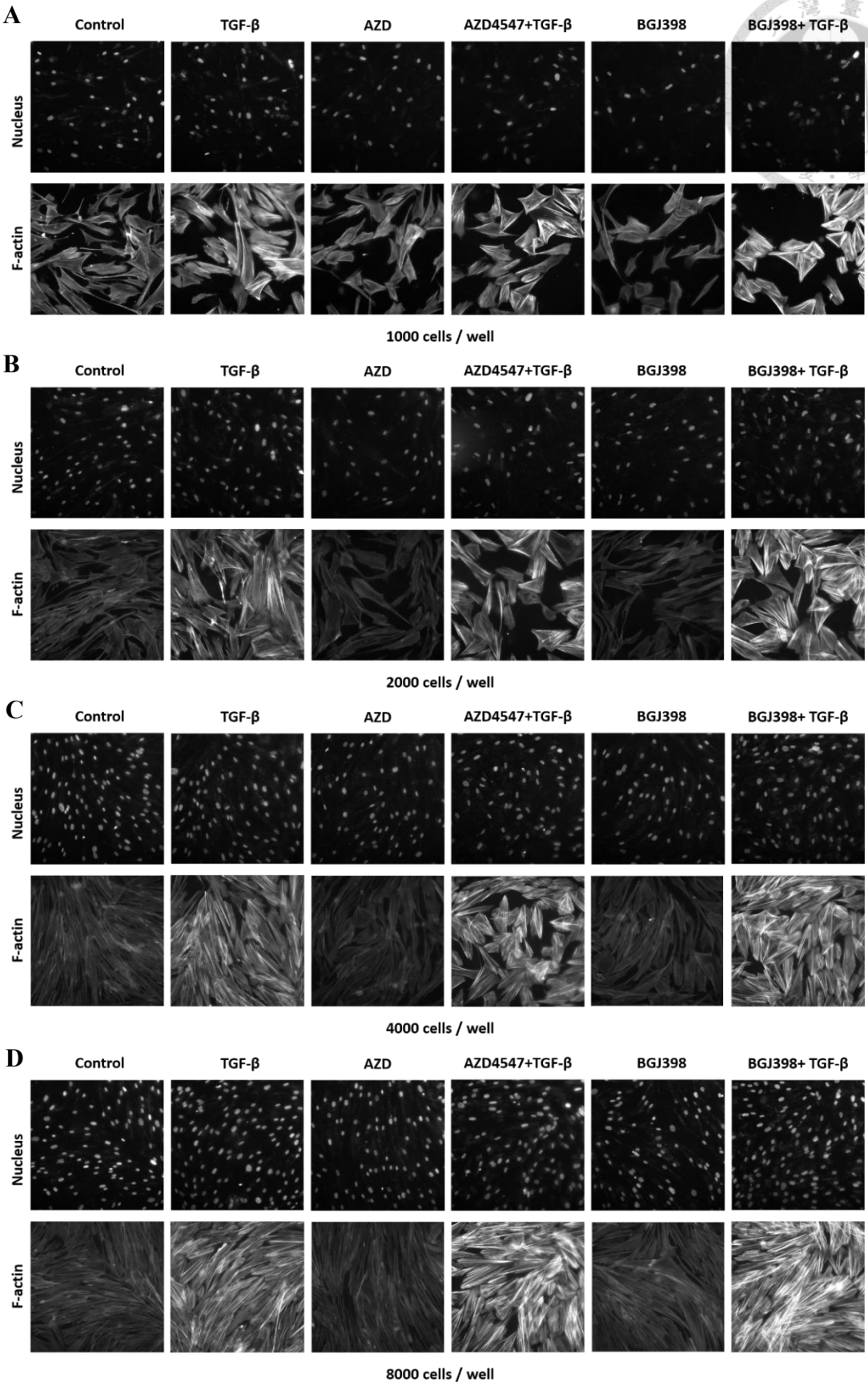

doi:10.6342/NTU202303790

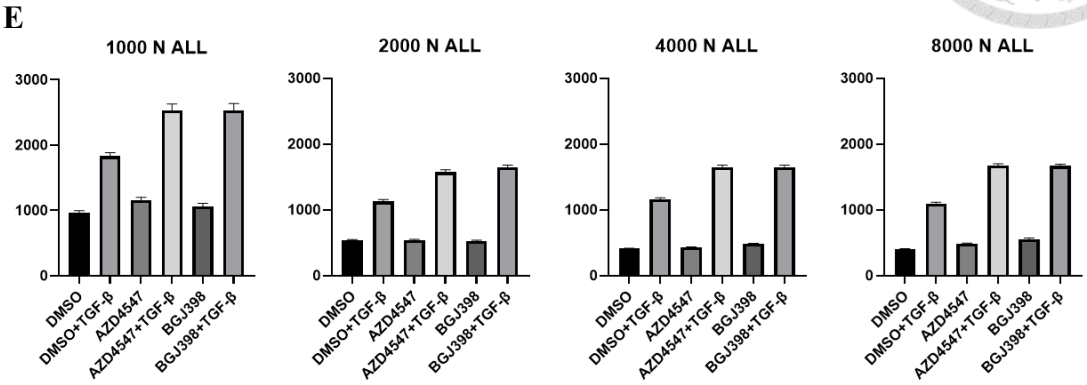

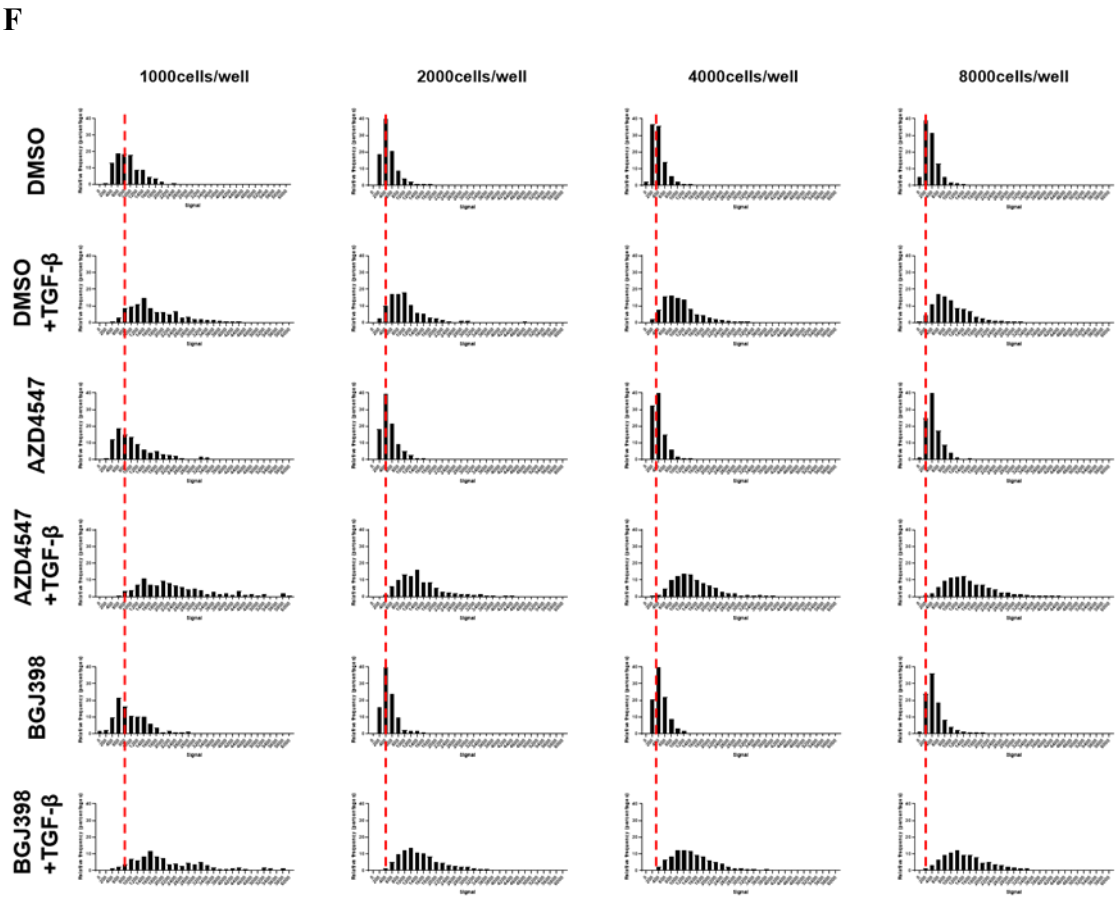

doi:10.6342/NTU202303790

Figure 11 Cytoskeleton remodeling was enhanced by TGF-β stimulation and FGFR kinase inhibitors but suppressed by high density-induced contact-inhibition in HS68 fibroblast cells

Phalloidin staining was performed to label actin cytoskeleton (A-D) Representative images of HS68 cells plated at the density of 1000/ 2000/ 4000/ 8000 cells per well and treated with DMSO, TGF-β or FGFR kinase inhibitors AZD4547 and BGJ398. Actin cytoskeleton decreased when cell density increased and TGF-β or TGF-β plus FGFR kinase inhibitors could further increase the filament structure. (E) Quantification of N signal based on MATLAB code. Noticed that high density- induced contact inhibition could be reversed by TGF-β or TGF-β plus FGFR kinase inhibitors. (F) Histograms of N signal in each group indicated that TGF-β induce an overall shift corresponding to observation of potent actin component on immunofluorescence images.

doi:10.6342/NTU202303790

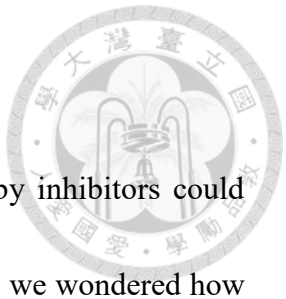

The data suggested that inhibition of FGFR kinase activity by inhibitors could further enhance TGF-β-induced actin cytoskeleton remodeling. Next, we wondered how actin dynamics of cells lost FGR1 receptor would respond to TGF-β stimulus. Again, phalloidin staining was performed on cells infected with shFGR1 lentivirus and treated with/without TGF-β or FGFR kinase inhibitors to see the effect of losing physical existence of FGFR1 on the phenotype. Similar to what we observed in Figure 11, shLuc and shFGFR1 groups both exhibited contact inhibition when cell density increased (Figure 12A to D). Cells treated with shLuc had an almost identical actin phenotypes to their naïve counterpart described in Figure 11. In contrast, knockdown of FGFR1 receptor resulted in an entirety decline of actin filament, with TGF-β could obviously increase the signal. The discrepancy of actin signal between shFGFR1 and shFGFR1 plus TGF-β was significantly higher than that between shLuc and shLuc plus TGF-β. This disparity suggested that besides kinase activity, FGFR1 receptor itself severed as important role on cytoskeleton remodeling coupling with activation of TGFβR signaling. TGF-β-induced signal shift was observed in FGFR1 knockdown group as well (Figure 12E).

doi:10.6342/NTU202303790

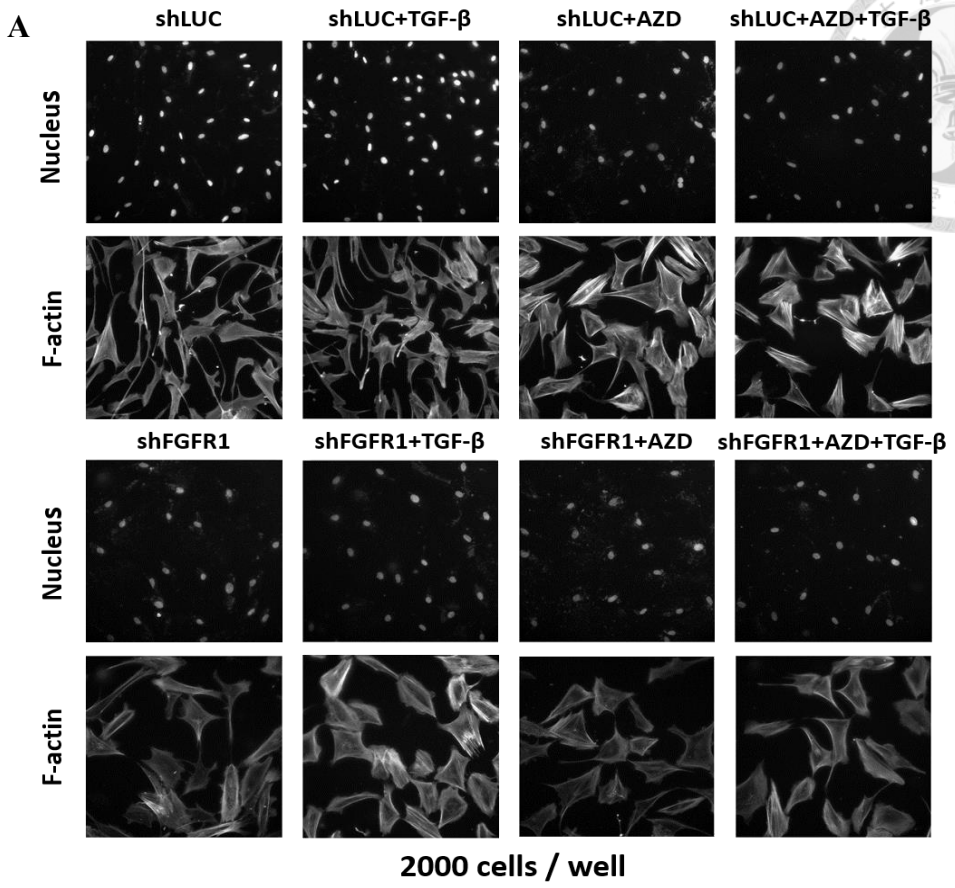

doi:10.6342/NTU202303790

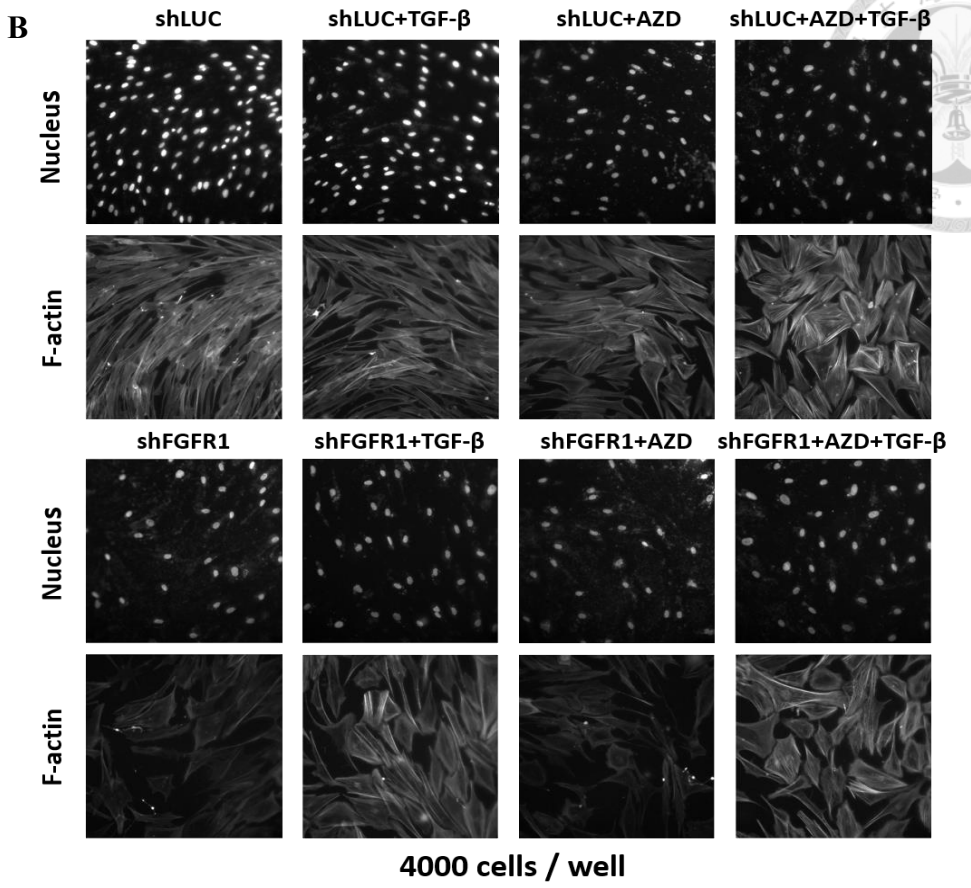

doi:10.6342/NTU202303790

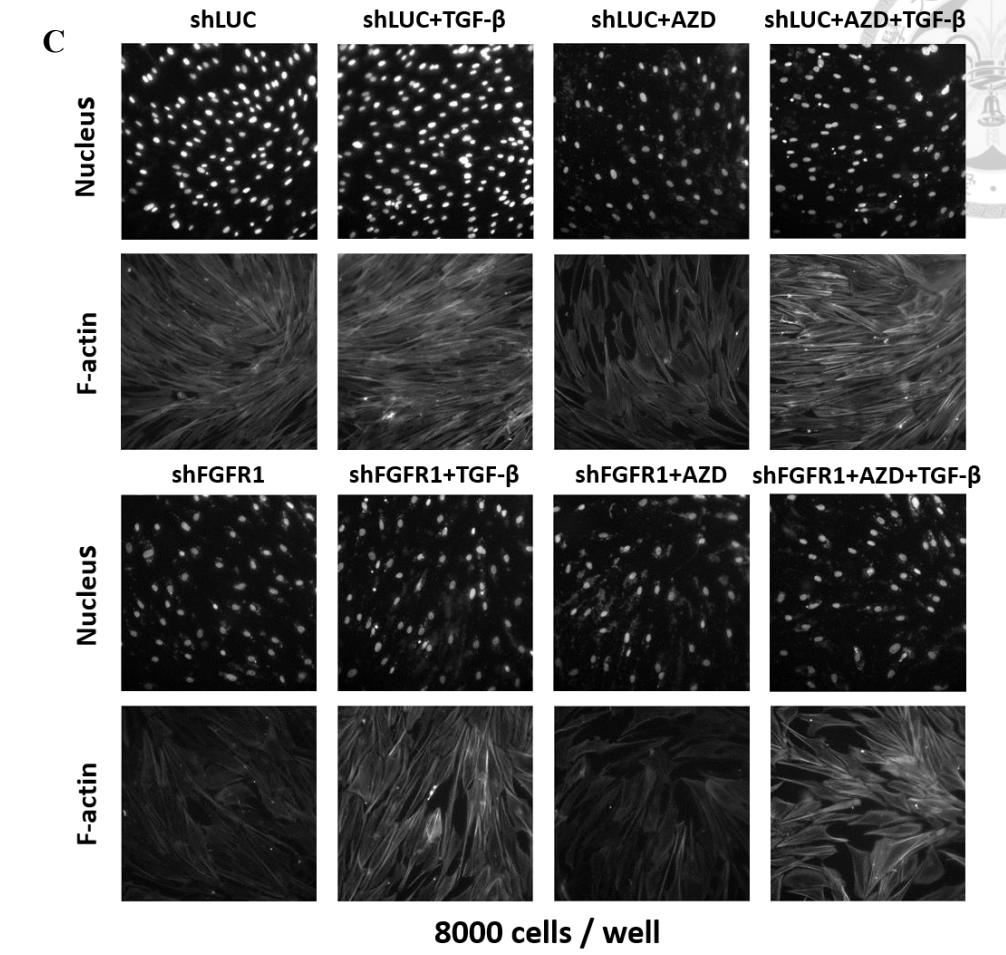

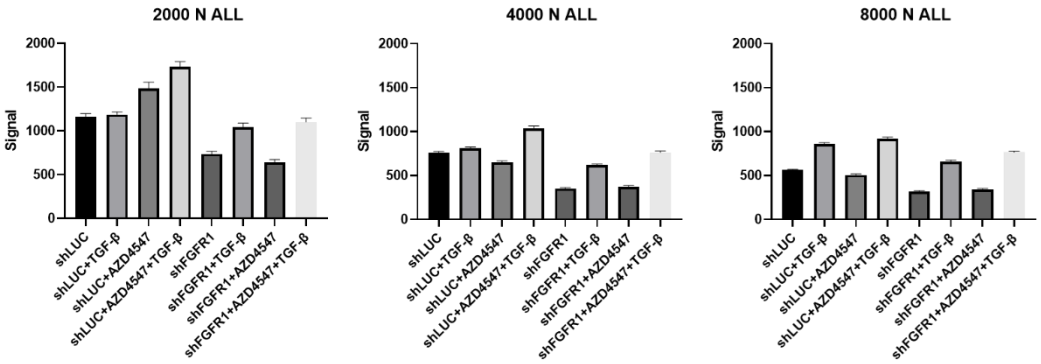

doi:10.6342/NTU202303790

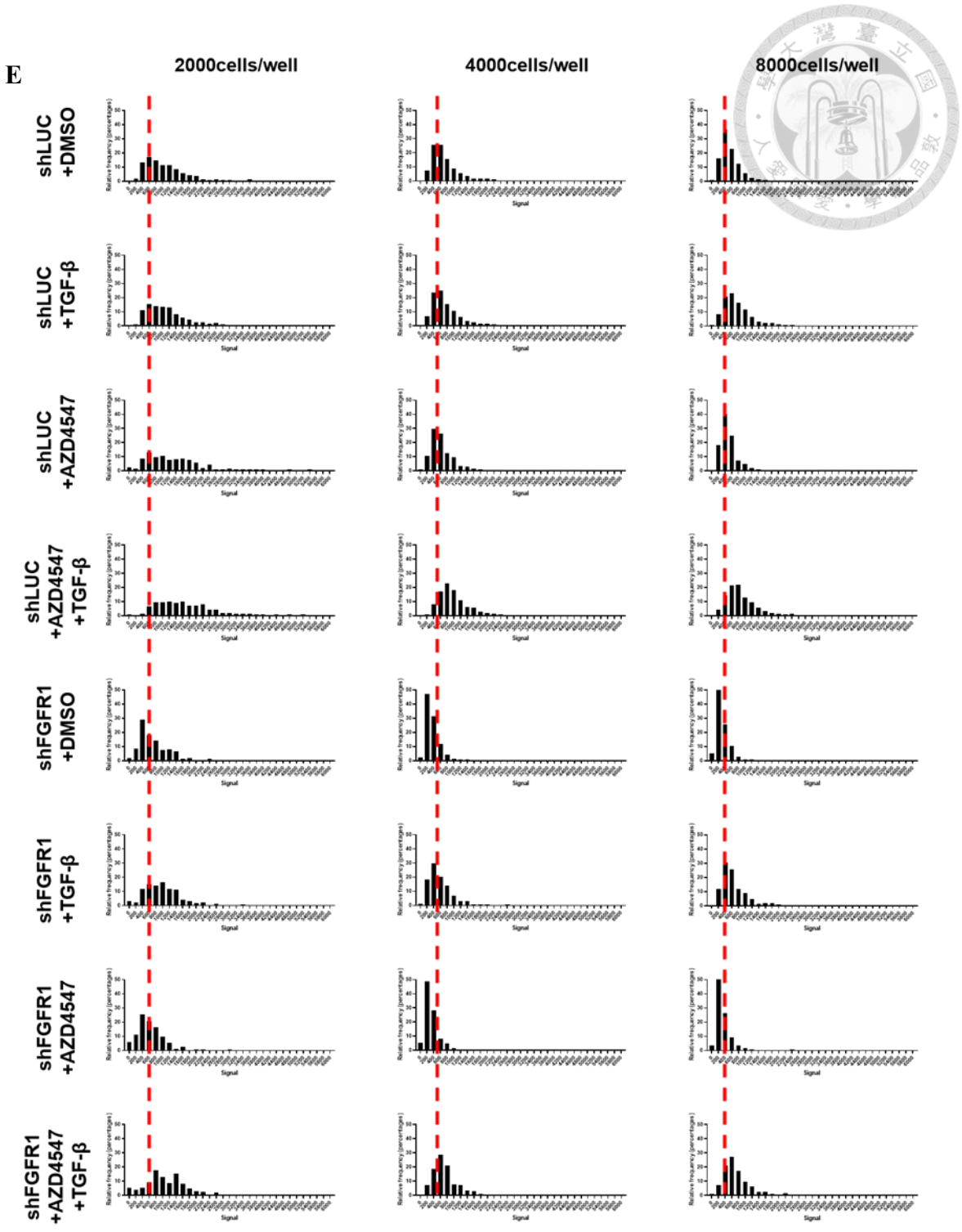

doi:10.6342/NTU202303790

Figure 12 FGFR1 knockdown greatly attenuated actin remodeling

Phalloidin staining was performed to label actin cytoskeleton (A-C) Representative images of HS68 cells grown at the density of 2000/ 4000/ 8000 cells in each 96 well, infected with lentivirus shLuc or shFGFR1 and then treated with DMSO, TGF-β or FGFR kinase inhibitors AZD4547 and BGJ398. Similarly, actin signal decreased when cell density increased and TGF-β induced the fiber pattern. The co-treatment of TGF-β and FGFR kinase inhibitors could further enhanced the signal in shLuc group, while not in shFGFR1 group due to loss of FGFR1 from cells. (D) Quantification of N signal based on MATLAB code. High density- induced contact inhibition could be reversed by TGF-β or TGF-β plus FGFR kinase inhibitors in shLuc group, with the latter combination exhibited greater enhancement. In shFGFR1 group, FGFR kinase inhibitors did not expedite more actin remodeling since their drug target was lost. (E) Histograms of N signal in each group indicated that TGF-β induce shift corresponding to immunofluorescence findings.

doi:10.6342/NTU202303790

Chapter 4 Discussion

In the study, we discovered that FGFR signaling had great impact on TGFβR-induced fibrotic event on HS68 fibroblast cells. FGFR kinase blockade increased TGF-β-induced formation of stress fibrous structure and α-SMA protein expression. Additionally, actin cytoskeleton remodeling was also enhanced by TGF-β upon FGFR kinase blockade. However, knockdown of FGFR1 receptor increased stress fiber but reduced α-SMA protein expression and cytoskeleton remodeling, indicating a complex manner of FGFR acting on TGFβR signaling.

4.1 TGF-β alone induced imperceptible stress fiber in HS68 fibroblast

We observed that cells incubated with TGF-β alone or TGF-β, FGF1 and FGFR kinase inhibitors together formed stress fiber in varying degrees (Figure 5). This discrepancy of fiber formation prompted us an assumption: In HS68 fibroblast cells there had a dominant endogenous FGFR signaling even when additional FGF stimulus was absent. This endogenous FGFR signaling is strong enough to minimize the contribution of exogenous TGF-β stimulus on constituting fiber structure and only administration of potent exogenous kinase inhibitors AZD4547 and BGJ398 could relieve this inhibiting

doi:10.6342/NTU202303790

effect. The combination of this kinase inhibitors and TGF-β create an optimal microenvironment, where TGF-β severed as strong fibrotic driver and these inhibitors further emancipate the restriction generated by kinase activity of FGFR.

4.2 Protein level of FGFR1 and TGFβR1 receptors were regulated precisely and spatiotemporally

In order to prevent constitutive activation, most of the membrane receptors undergoes some degrees of downregulation by several mechanisms to minimize the ligand-receptor binding event. For examples, upon activation of receptor tyrosine kinases via ligand stimulation these receptors may go through endocytosis to strictly regulate the signaling duration and downstream cascade. Meanwhile observing α-SMA protein expression under activation of FGFR1 or TGFβR signaling, we also wondered whether these two receptors showed some extent of regulations. Using immunoblotting, we observed that FGFR1 level was decreased when the cells stimulated by TGF-β. Moreover, prolonged TGF-β induction (96 hours of drug treatment) exhibited more decline compared to 48 hours of TGF-β induction (Figure 13). This finding was corresponding to the fact that more α-SMA protein was detected form 96 hours treatment group. On the

doi:10.6342/NTU202303790

other hand, level of TGFβR displayed another aspect of expression regulation. In 48 hours TGF-β treatment group, TGFβR level was elevated when FGFR kinase inhibitor existed in medium, while after 96 hours TGF-β treatment the protein exhibited greatly reduction responding to FGFR kinase blockade and TGF-β stimulation.

A

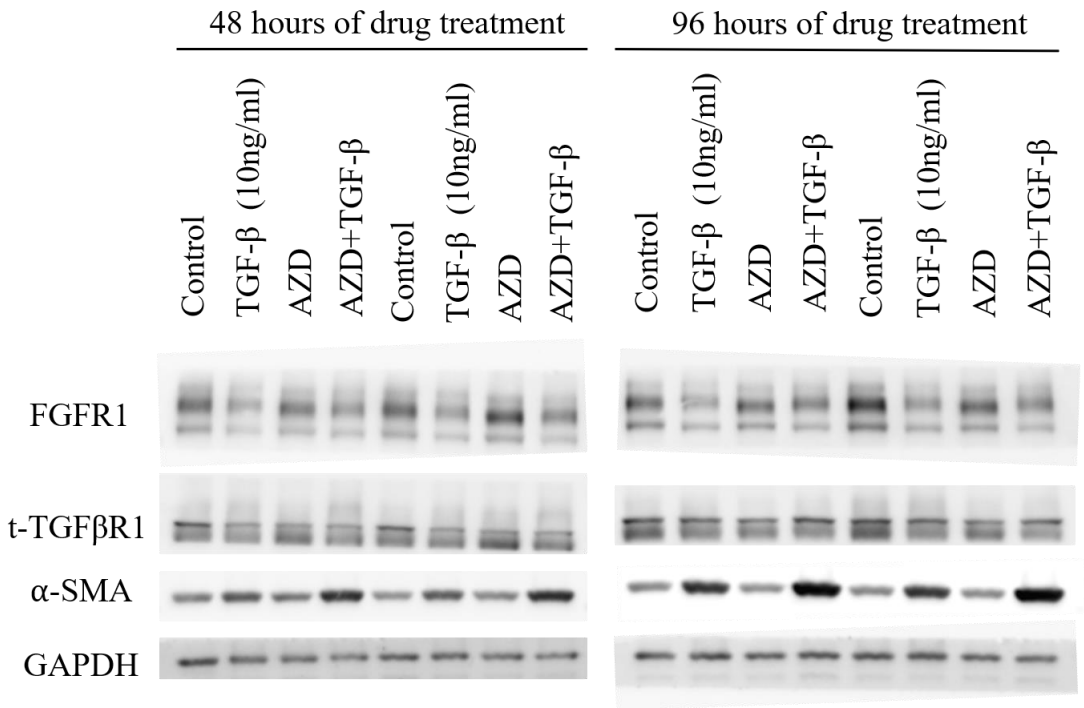

doi:10.6342/NTU202303790

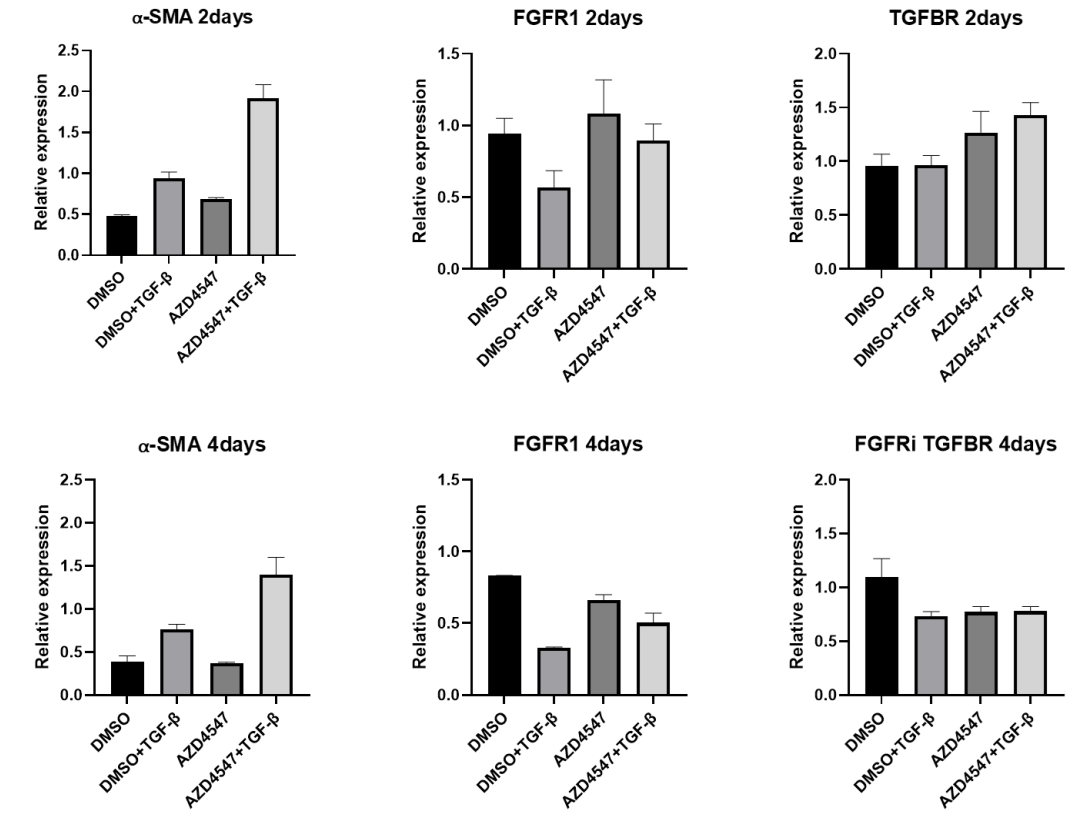

Figure 13 FGFR1 and TGFβR1 receptors exhibited distinct expression pattern in different timepoints.

(A) Hs68 fibroblasts were treated with TGF-β within control DMSO, FGFR inhibitors AZD4574 or BGJ398 background for 48 hours or 96 hours, respectively. Protein expression was analyzed by western blot. GAPDH was an internal control.

(B) Quantified α-SMA, FGFR1 and TGFβR1 signal from 48 hours or 96 hours group were plotted based on the relative level of α-SMA to GAPDH.

doi:10.6342/NTU202303790

4.3 Quantification of stress fiber signal based on relative threshold of immunofluorescence signal

To quantify the intensity of stress fiber induced by TGF-β, we first developed a MATLAB code to achieve this issue. Simply, this code calculated all α-SMA signal detected from each site of immunofluorescence images. However, it turned out that the quantification results indicating fiber intensity decreased after treatment of fibrotic driver TGF-β (Figure 14). This undesired result may be a consequence of our non-selective strategy, which captured total α-SMA signal instead of real α-SMA signal on stress fiber. We then modified this code to better quantify the "real fiber" signal, by performing blurring to the original images and setting the radius of pixels wielder. Theoretically, this modification not only allowed fibrous superstructure to be easily recognized, also excluded the most junk signal around fiber. Still, this approach failed since the code gave TGF-β group a lower fiber intensity than DMSO group. We noticed that compared to original code, the quantified results by fiber-specialized code showed higher fiber intensity in cells incubated with TGF-β plus FGFR kinase inhibitors group, indicating that the modification achieve some sort of intention we expected (Figure 14).

doi:10.6342/NTU202303790

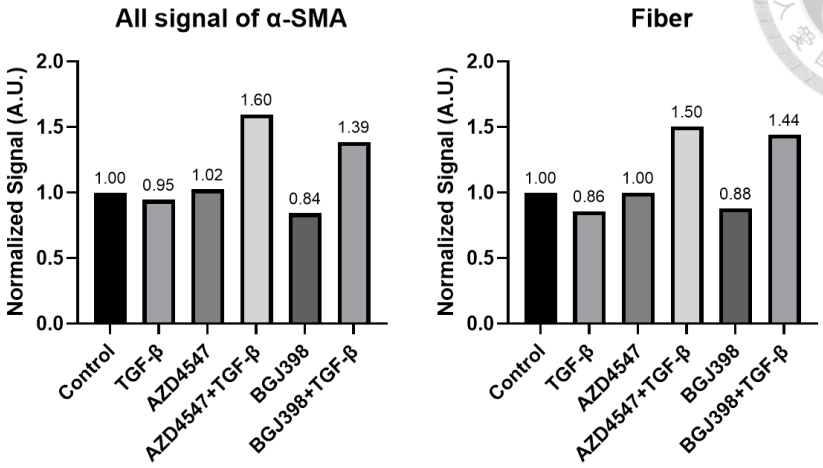

Figure 14 Quantification of total α-SMA signal or signal form fiber like pattern by MATLAB code

The MATLAB code was used to identify fiber intensity, with two approaches were used. One is to simply calculate all α-SMA signal from original images, the other one is to specifically capture signal form fiber-like structure after blurring the original images. However, these methods are all gave unreliable quantified results.

doi:10.6342/NTU202303790

4.4 Quantification of stress fiber signal based on its cellular distribution

The code used for actin cytoskeleton quantification in this study is originally used for other projects involving in counting lipid droplet. Sine this code is suitable for actin cytoskeleton quantification, we wondered if this code also fits on our intent goal of stress fiber analysis. N signal and C signal of α-SMA (details were described at Figure 10) were first calculated and then the ratio of them was further analyzed. Since N/C ratio implied the signal flow between nucleus and cytosol, we assumed that N/C ratio may be a valid indicator for stress fiber intensity.

We first examined the relationship between N and C signal of α-SMA on two - dimensional Cartesian coordinate system, by plotting N signal to y axis and C signal to x-axis to create scatter plots (Figure 15) Nevertheless, some mathematical issues happened on the scatterplot of N/C. We observed that he regression line of the N/C do not pass through the origin of coordinates (0,0) and plenty of discrete groups of points near the origin did exist (Figure 15A). The latter had an impact on determination the former, with discreteness created uncertainty. We speculated the problems may be due to imperfect background subtraction due to natural characteristic of α-SMA staining that created relative frequent noises in cytosol area during potent acetone/methanol fixation.

doi:10.6342/NTU202303790

Next, we attempted to calculated the difference between N and C signal. By subtracting each other, we surmised the process could minimize the discrete values near the origin. Then the values of (N-C) and N or C were used to create (N-C)/C or (N-C)/N scatter plots by plotting N-C to y axis and N or C to x-axis, respectively. Furthermore, we compared the results of N-C/C and N-C/N. The scatter plots indicated that N-C/N approach minimize the number of discrete points near to zero, while N-C/C generated the same mathematical issue of discrete points close to zero (Figure 15B and C). So, we decided to choose the N-C/N ratio as an indicator for stress fiber quantification.

After examination by scatter plots, we plotted histograms based on N-C/N ratio. The histograms showed that cells treated with TGF-β have a trend of decreased N-C values, which cause the overall shift to the negatively at x axis (Figure 16). The cells treated with TGF-β plus AZD4547 or BGJ398 even exhibited more prominent shift, while cells treated with inhibitors alone didn't. These features were indeed similar to what we observed on immunofluorescence images by eyes. (Figure 6) Thus, we regarded N-C/N ratio may be a simple and valid method to evaluate fiber formation instead of the previous approach that intend to capture specific signal from fiber superstructure. Still, this N-C/N ratio method needs more data to validate its practicality.

doi:10.6342/NTU202303790

doi:10.6342/NTU202303790

B

doi:10.6342/NTU202303790

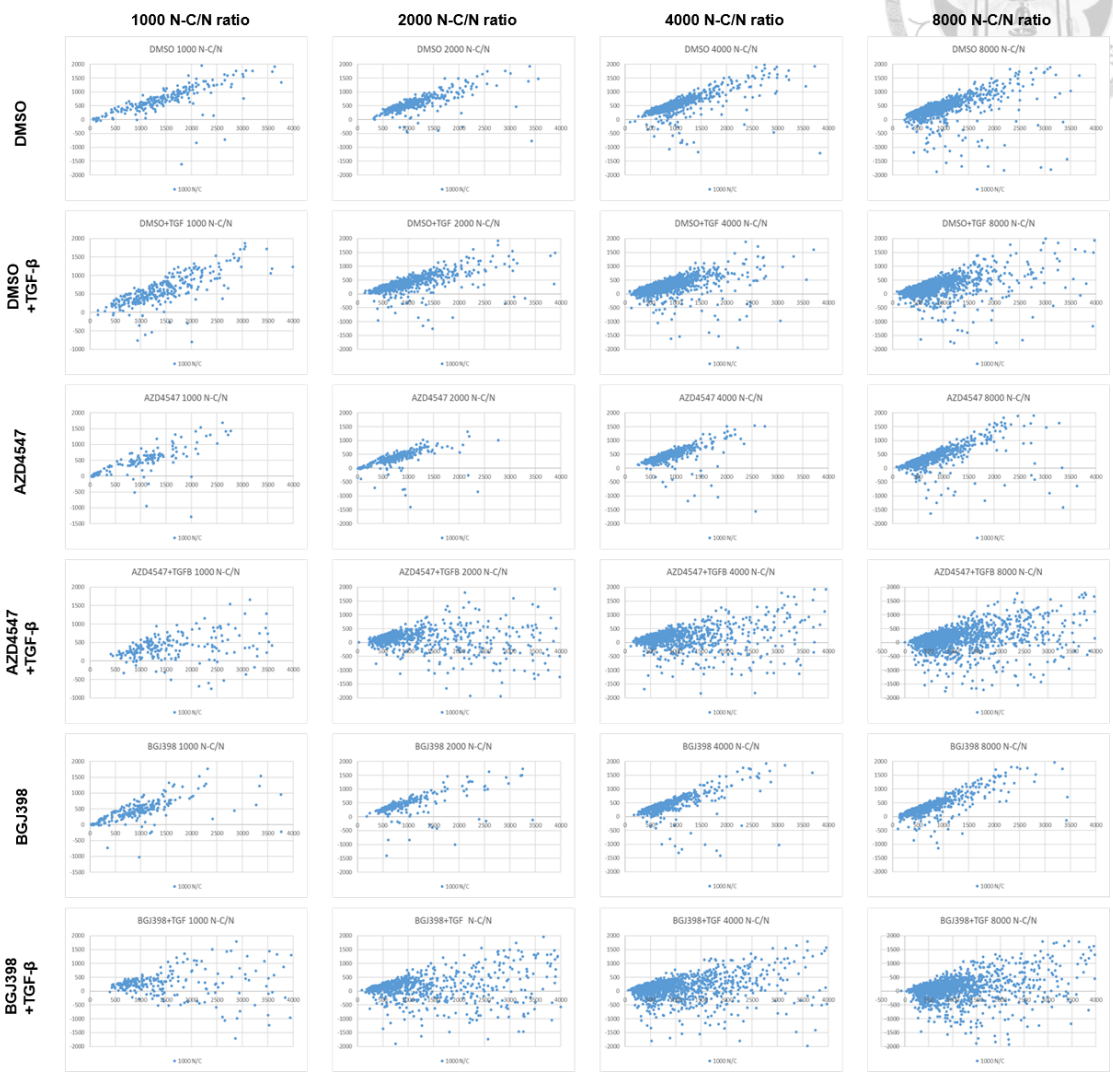

Figure 15 The scatterplots of N/C, (N-C)/C and (N-C)/N of α-SMA staining.

α-SMA staining was performed to label stress fiber. The N and C signal was calculated by code. Three different approaches N/C, (N-C)/C and (N-C)/N were plotted into scatter plot to distinguish the overall trend and examine whether potential mathematical issues that create uncertainty existed. Noticed that compared to (N-C)/N scatter plots (C), N/C,

doi:10.6342/NTU202303790

(N-C)/C scatter plots (A and B) exhibited some discrete values near the origin to some extent.

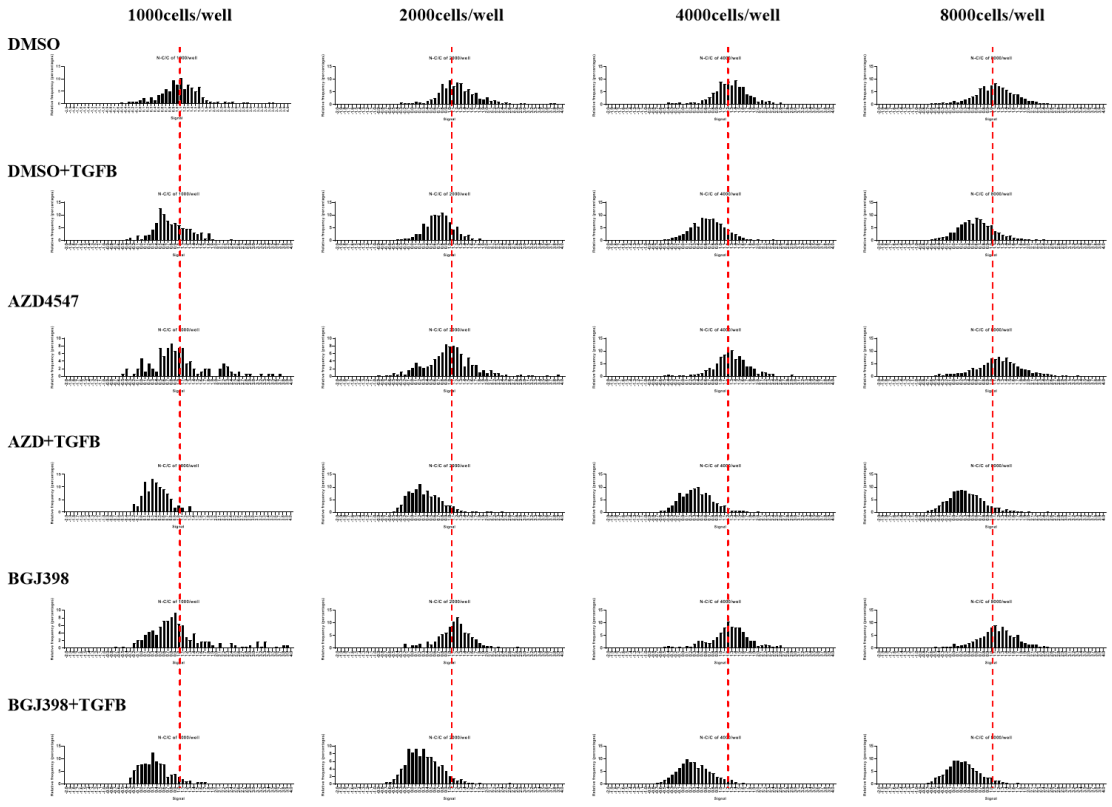

Figure 16 FGFR kinase inhibitors further promote the TGF-β induced- reduction of (N-C)/N ratio

The (N-C)/N ratios of each group were plotted as histograms. The results indicated that (N-C)/N ratio decreased after TGF-β treatment, with FGFR kinase inhibitors further enhanced this effect. While inhibitors alone did not result in any obvious signal shift compared to TGF-β or TGF-β plus inhibitors group.

doi:10.6342/NTU202303790

4.5 The discrepancy between immunoblotting and immunofluorescence

Immunoblotting indicated that α-SMA level reduced after loss of FGFR1, while immunofluorescence showed fiber still forms under same knock down treatment (Figure 7 and 8). We assumed that α-SMA stress fiber structure involves several cellular events that tightly linked together. Briefly, two aspect could be divided form fiber formation, one is the production of fiber component α-SMA protein and the other is the assembling of α-SMA protein to become stress fiber. Our immunoblotting data suggested that FGFR receptor is crucial for α-SMA protein level by some sort of mechanism. We listed 3 possible explanations to fit these finding:

Possibilities	The mechanisms
1. Transcription	FGFR receptor enhance transcription of α-SMA, while its kinase prevents overproducing of the protein as well
2. Protein stability	FGFR receptor could stabilize α-SMA protein from degradation via kinase independent manner
3. Transport inhibition	FGFR kinase activity prevent α-SMA protein to assemble to structure of stress fiber.

Table 2 The possible mechanisms how FGFR-mediated TGF-β signaling on stress fiber formation.

doi:10.6342/NTU202303790

In order to examine these assumptions, some specific techniques would be applied. The precise quantitative polymerase chain reaction (qPCR) could be performed to examine transcription patterns of α-SMA. And protein degradation assay based on translation-terminating agent cycloheximide could be used for verifying the stability of α-SMA protein. As for studying the weather transport inhibition of α-SMA into stress fiber via FGFR, we have tried to co-staining F-actin and α-SMA at the same time but failed. The α-SMA staining exclusively relied on methanol/acetone fixation, which would bring catastrophic deformation to the F-actin cytoskeleton and ultimately rejects phalloidin dye to bind within. To solve this technical issue, HS68 cell lines that constantly expressed fluorescent protein-tagged α-SMA or actin could be established.

doi:10.6342/NTU202303790

4.6 Effects of FGFR, TGFβR signaling and cell density on actin cytoskeleton remodeling on HS68 fibroblast cells

We observed that the high density of cells caused overall actin signal reduced, while combination of FGFR kinase blocked and TGF-β stimulus could reverse this inhibition. On the other hands, loss of FGFR1 receptor greatly reduced actin signal, and TGF-β stimulus could slightly rescue this effect. We then speculated the contact inhibition of actin cytoskeleton remodeling was contributed to FGFR kinase activity and FGFR receptor itself also regulate the formation of basal actin structure via kinase independent manner, which is similar to what we observed at α-SMA level form immunoblotting data.

We are currently infected HS68 cells for overexpressing wildtype FGFR1 and its kinase dead versions (D623A and Y653/654F). By performing overexpression experiment, we could further validate our assumption that full-functioning FGFR1 and FGFR1 without kinase activity have distinct effects on actin cytoskeleton remodeling and stress fiber formation.

doi:10.6342/NTU202303790

Chapter 5 Conclusion

We performed several immunofluorescences and immunoblotting on HS68 fibroblast model to elucidate how TGFβR and FGFR signaling regulating fibroblast differentiation. We also observed that TGF-β-induced actin remodeling and high density-induced contact inhibition on fibroblasts were precisely regulated by FGFR as well. These findings suggested that FGFR may mediate TGFβR signaling in kinase-dependent and kinase-independent manners concomitantly.

FGFR and TGFβR signaling are both play a crucial role on fibroblast functionalities in vivo and in vitro. We are looking forward to understand the molecular mechanisms how these two signaling interact and crosstalk upon their activation and wish to develop powerful FGFR-TGFβR targeting therapy to treat TED.

doi:10.6342/NTU202303790

Chapter 6 References

1. Menconi, F., C. Marcocci, and M. Marinò, *Diagnosis and classification of Graves' disease.* Autoimmunity Reviews, 2014. **13**(4): p. 398-402.
2. McIver, B. and J.C. Morris, *THE PATHOGENESIS OF GRAVES' DISEASE.* Endocrinology and Metabolism Clinics of North America, 1998. **27**(1): p. 73-89.
3. Antonelli, A., et al., *Graves' disease: Clinical manifestations, immune pathogenesis (cytokines and chemokines) and therapy.* Best Practice & Research Clinical Endocrinology & Metabolism, 2020. **34**(1): p. 101388.
4. Douglas, R.S. and S. Gupta, *The pathophysiology of thyroid eye disease: implications for immunotherapy.* Curr Opin Ophthalmol, 2011. **22**(5): p. 385-90.
5. Chin, Y.H., et al., *Prevalence of thyroid eye disease in Graves' disease: A meta-analysis and systematic review.* Clinical Endocrinology, 2020. **93**(4): p. 363-374.
6. Şahlı, E. and K. Gündüz, *Thyroid-associated Ophthalmopathy.* Turk J Ophthalmol, 2017. **47**(2): p. 94-105.
7. Yoon, J.S. and D.O. Kikkawa, *Thyroid eye disease: From pathogenesis to targeted therapies.* Taiwan J Ophthalmol, 2022. **12**(1): p. 3-11.
8. Cockerham, K.P., et al., *Correction to: Quality of Life in Patients with Chronic Thyroid Eye Disease in the United States.* Ophthalmology and Therapy, 2022.

doi:10.6342/NTU202303790

11(2): p. 923-923.

9. Bartalena, L., et al., *The 2016 European Thyroid Association/European Group on Graves' Orbitopathy Guidelines for the Management of Graves' Orbitopathy.* European Thyroid Journal, 2016. **5**(1): p. 9-26.

10. Jain, A.P., P. Jaru-Ampornpan, and R.S. Douglas, *Thyroid eye disease: Redefining its management—A review.* Clinical & Experimental Ophthalmology, 2021. **49**(2): p. 203-211.

11. Phillips, M.E., M.M. Marzban, and S.S. Kathuria, *Treatment of Thyroid Eye Disease.* Current Treatment Options in Neurology, 2010. **12**(1): p. 64-69.

12. Naik, M.N., et al., *Minimally invasive surgery for thyroid eye disease.* Indian J Ophthalmol, 2015. **63**(11): p. 847-53.

13. Kumar, S., et al., *Evidence for enhanced adipogenesis in the orbits of patients with Graves' ophthalmopathy.* J Clin Endocrinol Metab, 2004. **89**(2): p. 930-5.

14. Ludgate, M., *Fibrosis in dysthyroid eye disease.* Eye (Lond), 2020. **34**(2): p. 279-284.

15. Du, Z. and C.M. Lovly, *Mechanisms of receptor tyrosine kinase activation in cancer.* Molecular Cancer, 2018. **17**(1): p. 58.

16. McDonell, L.M., et al., *Receptor tyrosine kinase mutations in developmental*

doi:10.6342/NTU202303790

syndromes and cancer: two sides of the same coin. Hum Mol Genet, 2015. **24**(R1): p. R60-6.

17. Wong, L. L., N. G. Lee, D. Amarnani, C. J. Choi, D. R. Bielenberg, S. K. Freitag, P. A. D'Amore, and L. A. Kim. 2016. 'Orbital Angiogenesis and Lymphangiogenesis in Thyroid Eye Disease: An Analysis of Vascular Growth Factors with Clinical Correlation', *Ophthalmology*, 123: 2028-36.

18. Cheng, Lu, Jing Hu, Ling Zhang, Ning Shen, Hui Chen, and Fang Zhang. 2022. 'Repurposing Lenvatinib as A Potential Therapeutic Agent against Thyroid Eye Disease by Suppressing Adipogenesis in Orbital Adipose Tissues', *Pharmaceuticals*, 15: 1305.

19. Porębska, N., et al. *Targeting Cellular Trafficking of Fibroblast Growth Factor Receptors as a Strategy for Selective Cancer Treatment*. Journal of Clinical Medicine, 2019. **8**, DOI: 10.3390/jcm8010007.

20 Zhao, M., L. Wang, M. Wang, S. Zhou, Y. Lu, H. Cui, A. C. Racanelli, L. Zhang, T. Ye, B. Ding, B. Zhang, J. Yang, and Y. Yao. 2022. 'Targeting fibrosis, mechanisms and cilinical trials', *Signal Transduct Target Ther*, 7: 206.

21 D'Urso, M., and N. A. Kurniawan. 2020. 'Mechanical and Physical Regulation of Fibroblast-Myofibroblast Transition: From Cellular Mechanoresponse to Tissue

Pathology', *Front Bioeng Biotechnol*, 8: 609653.

22 Xie, Bingyu, Wei Xiong, Feng Zhang, Nuo Wang, Yong Luo, Yizhi Chen, Jiamin Cao, Zhuokun Chen, Chen Ma, and Haiyan Chen. 2023. 'The miR-103a-3p/TGFBR3 axis regulates TGF-β-induced orbital fibroblast activation and fibrosis in thyroid-eye disease', *Molecular and Cellular Endocrinology*, 559: 111780.

23 Krieger, Christine C. 2021. 'The Forks in the Road of Thyroid Eye Disease', *The Journal of Clinical Endocrinology & Metabolism*, 106: e5262-e63.

24. Shi, X., et al., *Transforming Growth Factor-β Signaling in Fibrotic Diseases and Cancer-Associated Fibroblasts.* Biomolecules, 2020. **10**(12).

25. Meng, X.-m., D.J. Nikolic-Paterson, and H.Y. Lan, *TGF-β: the master regulator of fibrosis.* Nature Reviews Nephrology, 2016. **12**(6): p. 325-338.

26. Chen, P.-Y., et al., *FGF Regulates TGF-β Signaling and Endothelial-to-Mesenchymal Transition via Control of let-7 miRNA Expression.* Cell Reports, 2012. **2**(6): p. 1684-1696.

27. Kobashigawa, Yoshihiro, Shinjiro Amano, Mariko Yokogawa, Hiroyuki Kumeta, Hiroshi Morioka, Masayori Inouye, Joseph Schlessinger, and Fuyuhiko Inagaki. 2015. 'Structural analysis of the mechanism of phosphorylation of a

doi:10.6342/NTU202303790

critical autoregulatory tyrosine residue in FGFR1 kinase domain', *Genes to Cells*, 20: 860-70.

28. Lew, E. D., C. M. Furdui, K. S. Anderson, and J. Schlessinger. 2009. 'The precise sequence of FGF receptor autophosphorylation is kinetically driven and is disrupted by oncogenic mutations', *Sci Signal*, 2: ra6.

29. Sandbo, N., and N. Dulin. 2011. 'Actin cytoskeleton in myofibroblast differentiation: ultrastructure defining form and driving function', *Transl Res*, 158: 181-96.

30. Fernáandez-Borja, Mar, David Bellido, Ricardo Makiya, Guido David, Gunilla Olivecrona, Manuel Reina, and Senén Vilaró. 1995. 'Actin cytoskeleton of fibroblasts organizes surface proteoglycans that bind basic fibroblast growth factor and lipoprotein lipase', *Cell Motility*, 30: 89-107.

31. Egan, J. J., G. Gronowicz, and G. A. Rodan. 1991. 'Cell density-dependent decrease in cytoskeletal actin and myosin in cultured osteoblastic cells: correlation with cyclic AMP changes', *J Cell Biochem*, 45: 93-100.

32. Schmitt-Ney, Michel, and Joel F. Habener. 2004. 'Cell-density-dependent regulation of actin gene expression due to changes in actin treadmilling', *Experimental Cell Research*, 295: 236-44.

doi:10.6342/NTU202303790

Chapter 7 Supplementary information

7.1 Maps of FGFR1 overexpression constructs

Construct of FGFR1 overexpression plasmid

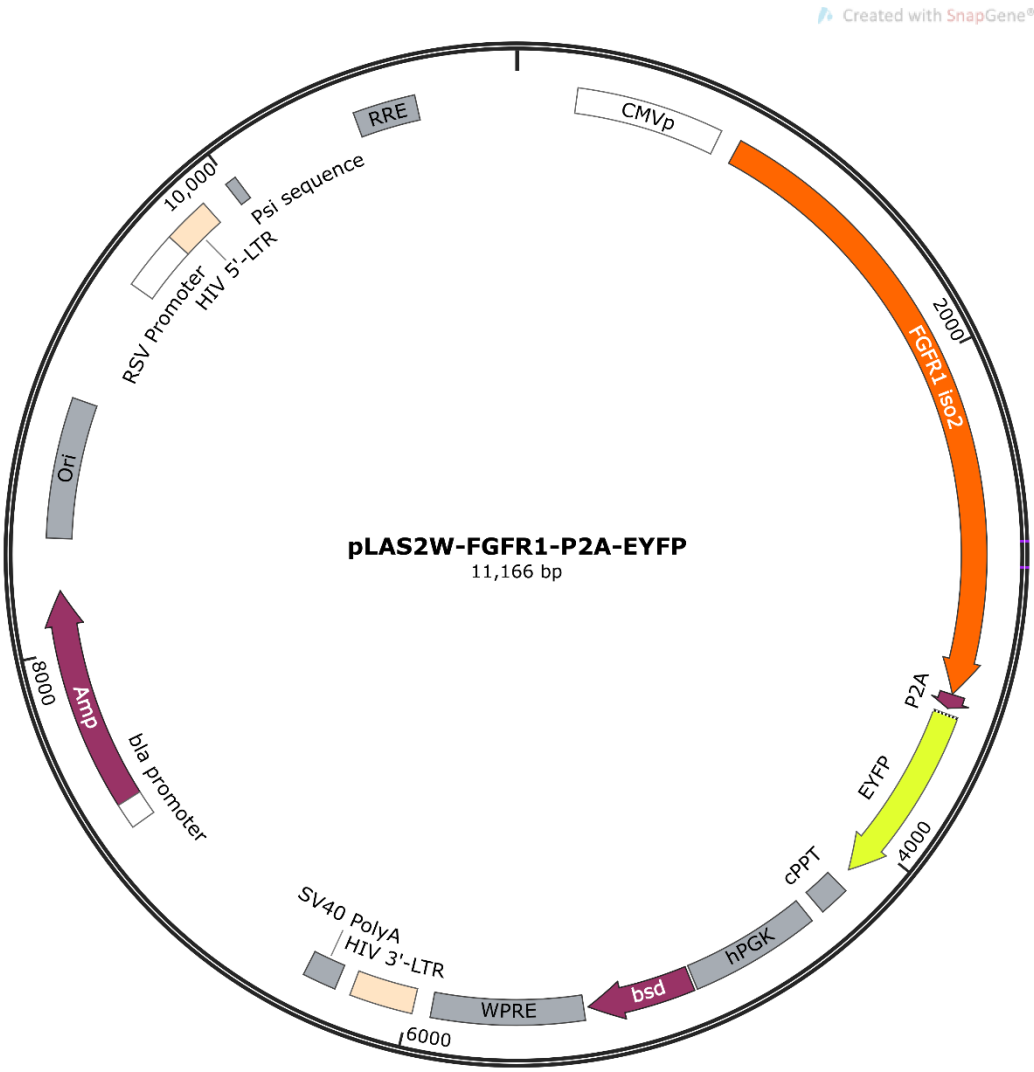

doi:10.6342/NTU202303790

Construct of kinase-dead FGFR1 (D623A) overexpression plasmid

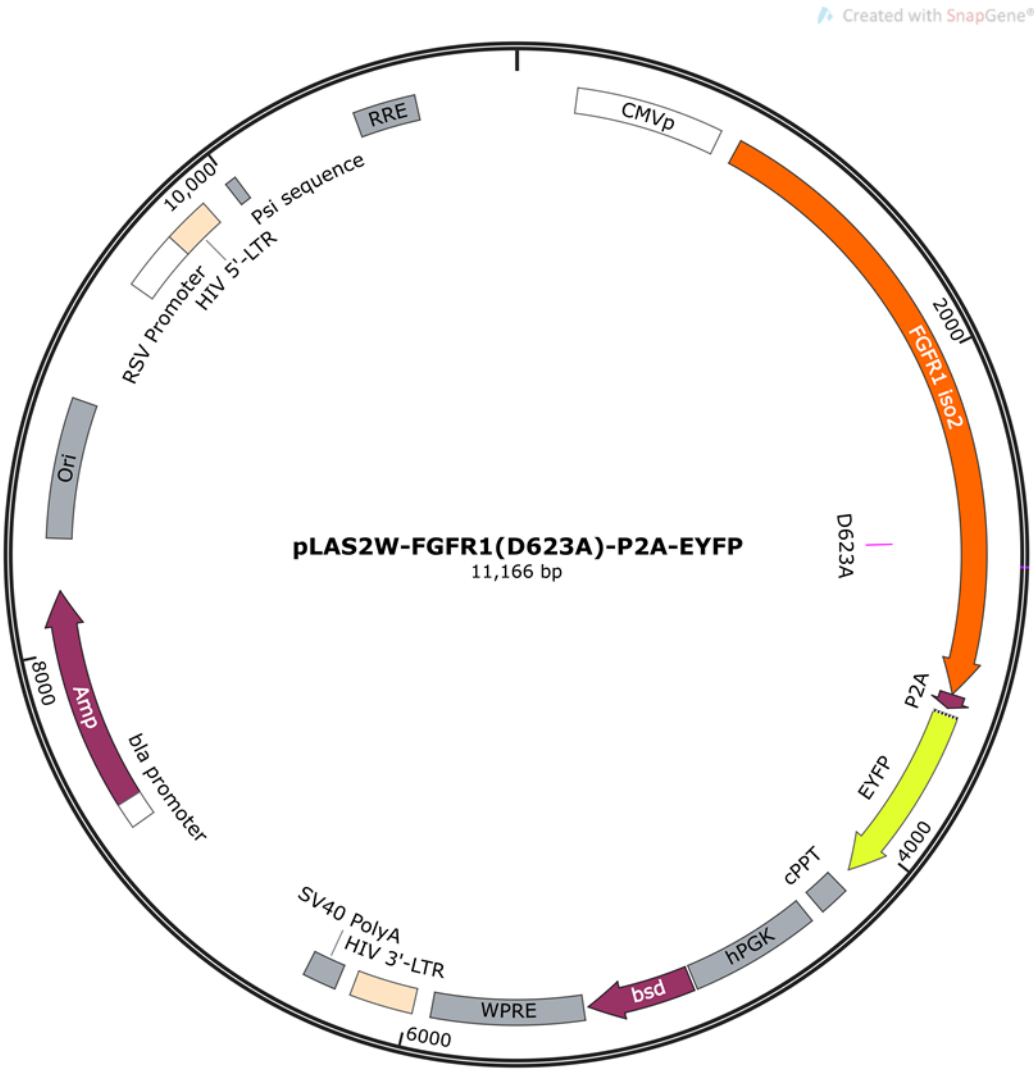

doi:10.6342/NTU202303790

Construct of kinase-dead FGFR1 (Y653/654F) overexpression plasmid

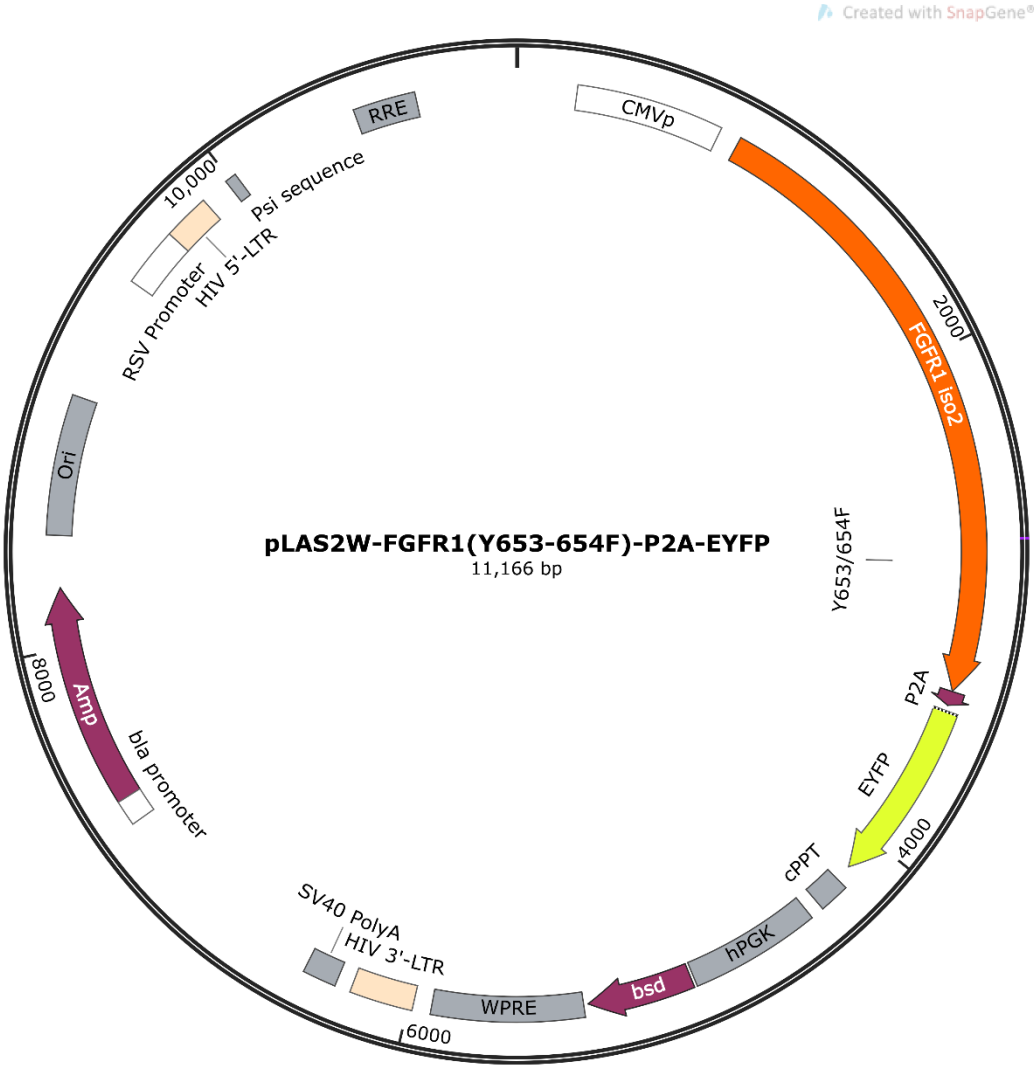

doi:10.6342/NTU202303790

7.2 MATLAB scripts

save_fluoref_cor_img_for_IF_20210804_lin

(Fluo correction of ND2 files for stress fiber quantification)

```
%%

close all;clc;clear mex;clear;

cwd='E:\20221010 HS68 KD FGFR1 TGF\shFGFR1 TGF\';cd(cwd)

%cfolder='';

mkdir([cwd,'fluo_corrected/']);

%% fluo reference

c_off=single(imresize(imread([cwd,'\fluo_reference\off.tif']),1));

c_on{1}=single(imresize(imread([cwd,'\fluo_reference\dapi.tif']),1));

%c_on{2}=single(imresize(imread([cwd,'\fluo_reference\fitc.tif']),1));

c_on{2}=single(imresize(imread([cwd,'\fluo_reference\txred.tif']),1));

c_ref=cellfun(@(x) (x-c_off),c_on,'UniformOutput',false);

c_mean=cellfun(@(x) mean((x-c_off),'All'),c_on);



%% import multiple ND file
```


doi:10.6342/NTU202303790

```
 dir_name=dir([cwd,'*.nd2']);
 wellname=arrayfun(@(x)
extractBefore(x.name,'.nd2'),dir_name,'UniformOutput',false);

 for ii=1:size(dir_name,1)
        data=bfGetReader([cwd,dir_name(ii).name],0);
        xynum=data.getSeriesCount();
        tnum=data.getSizeT();
        znum=data.getSizeZ();
        cnum=data.getSizeC();
        %fprintf(['xy number= ',num2str(xynum),'; frame number= ',num2str(tnum),'; z
number= ',num2str(znum)])
        cimage_cr={};
        %% correct image
        for xy=1:xynum
            tic
            data.setSeries(xy-1);
            %cimage_ori={};
```


doi:10.6342/NTU202303790

```
for tt=1:tnum
    %                   close all;
    for cc=1:cnum
        for zz=1:znum

disp([wellname{ii},'xy',num2str(xy),'t',num2str(tt),'c',num2str(cc),'z',num2str(zz)])
                    iPlane = data.getIndex(zz-1,cc-1,tt-1)+1; %iPlane =
reader.getIndex(iZ - 1, iC -1, iT - 1) + 1;
                    img = bfGetPlane(data, iPlane);
                    s_img=single(img);
                    %cimage_ori{tt,cc}=img;
                    cimage_cr{xy,cc}{zz}=((s_img-
c_off)./c_ref{cc}*c_mean(cc));
                    %cimage_cr{tt,1}=((s_img-c_off)./c_ref{cc}*c_mean(cc));
                    %% demo fluo_corrected image
                    %                   if tt==1
                    %
cscale{cc}=prctile(cimage_cr{tt,cc}{1}(:),[0.001 99.999]);
```


doi:10.6342/NTU202303790

```
                    %                                   end

                    %

figure(cc*1000+zz);set(gcf,'position',get(0,'ScreenSize'))

                    %                                   figure(cc*1000+zz);hold

off;subplot(1,2,1);imagesc(cimage_ori{tt,cc}{zz});title(['Frame',num2str(cc),num2str(z

z)]);ylabel('non-corrected')

                    %                                                       hold

off;subplot(1,2,2);imagesc(cimage_cr{tt,cc}{zz},cscale{cc});ylabel('corrected')

                    %xy_num=['0',num2str(xy)];xy_num=xy_num(end-1:end);

                    %c_num=['0',num2str(cc)];c_num=c_num(end-1:end);

                    %z_num=['0',num2str(zz)];z_num=z_num(end-1:end);


%save([cwd,'fluo_corrected\',wellname{ii},'xy',xy_num,'c',c_num,'z',z_num,'.mat'],'cim

age_cr')


                end

            end

        end
```


doi:10.6342/NTU202303790

```
        end
        %% save image
        save([cwd,'fluo_corrected\',wellname{ii},'.mat'],'cimage_cr')
        toc
end


%% 驗證 大小


% cwd='H:\Lin\20210116_Cal27_KD_SLK\fluo_corrected\';
% dir_name=dir([cwd,'*.mat']);
%
% for ii=1:size(dir_name,1)
%         load([cwd,dir_name(ii).name]);
%         size_sz{ii,1}=size(cimage_cr);
% end
```


doi:10.6342/NTU202303790

Calc_asma_intensity_20220415

(Quantification of stress fiber signal based on relative threshold)

```
% 抓整張訊號
close all;clc;clear;
cwd='F:\20221010 HS68 KD FGFR1 TGF\shluc\'; cd(cwd);
mkdir('./celldata');
nucr=25;
%%
dir_name=dir([cwd,'fluo_corrected\','*.mat']);
% tempmtx=zeros(8,12);
% tempmtx_d=zeros(8,12);
% tempmtx_s=zeros(8,12);
% wellden=zeros(8,12);
%ascii_v=arrayfun(@(x)
extractBetween(x.name,'Well','.mat'),dir_name,'UniformOutput',false);
ascii_v=arrayfun(@(x) extractBefore(x.name,'_'),dir_name,'UniformOutput',false);
ascii_v2=arrayfun(@(x)                                    unicode2native(x,'US-
ASCII'),string(ascii_v),'UniformOutput',false);
```


doi:10.6342/NTU202303790

```
%%

group_name={};tempmtx_s=[];wellden=[];

tempmtx_fiber=[];tempmtx_all=[];

for ii=1:size(dir_name,1)

    tic

    row=(ascii_v2{ii}(1)-64);

    col=str2double(char(ascii_v2{ii}(2:3)));

    load([cwd,'fluo_corrected\',dir_name(ii).name],'cimage_cr')

    group_name_t=repmat({ascii_v{ii}},size(cimage_cr,1),1);

    group_name=[group_name;group_name_t];

    tempmtx_s_t2=[];wellden_t2=[];

    tempfiber=[];tempall=[];

    for xy=1:size(cimage_cr,1)

        % cimage_cr{xy,cc}(zz)

        nucimg_t=cimage_cr{xy,1};

        nucimg_t2=cell2mat(nucimg_t);
```


doi:10.6342/NTU202303790

```
nucimg_t2=reshape(nucimg_t2,size(nucimg_t{1,1},1),size(nucimg_t{1,1},2),size(nuci
mg_t,2));

        smaimg_t=cimage_cr{xy,2};

        smaimg_t2=cell2mat(smaimg_t);


smaimg_t2=reshape(smaimg_t2,size(smaimg_t{1,2},1),size(smaimg_t{1,2},2),size(sma
img_t,2));

        %       % sort

        %       disp('Sorting......')

        %       nucimg_t_sort=sort(nucimg_t2,3,'descend');

        %       nucimg_max=mean(nucimg_t_sort(:,:,1:3),3);

        %       smaimg_t_sort=sort(smaimg_t2,3,'descend');

        %       smaimg_max=mean(smaimg_t_sort(:,:,1:3),3);

        %       figure(100);subplot(1,2,1);imshow(sqrt(abs(nucimg_max)),[]);

        %       subplot(1,2,2);imshow(sqrt(abs(smaimg_max)),[]);

        %       title(ascii_v{ii});

        %       set(gcf, 'Position', get(0, 'Screensize'));
```


doi:10.6342/NTU202303790

```
% average
disp([dir_name(ii).name,'_xy',num2str(xy)])
z_focus=input('Focus z? (num) ');
nucimg_max=mean(nucimg_t2(:,:,:),3);
%smaimg_max=mean(smaimg_t2(:,:,:),3);
smaimg_max=smaimg_t2(:,:, z_focus);
figure(100);subplot(1,2,1);imshow(sqrt(abs(nucimg_max)),[]);title('DAPI')
subplot(1,2,2);imshow(sqrt(abs(smaimg_max)),[]);title('Original')
title([ascii_v{ii},'xy',num2str(xy)]);
set(gcf, 'Position', get(0, 'Screensize'));
%remove outliers
figure(101);hh = histogram(smaimg_max);
hhv = hh.Values;
tempimg_bl=imfilter(nucimg_max,fspecial('disk',2),'symmetric');
tempimg_bs=bgsub(tempimg_bl,3*nucr,0);
[~,~,bgn]=ThreshImage(tempimg_bs);tempimg_bs=tempimg_bs-bgn;
tempimg_bl2=imfilter(smaimg_max,fspecial('disk',2),'symmetric');     %  會
```

部會模糊過頭了?

doi:10.6342/NTU202303790

```
figure(200);subplot(1,2,1);imshow(sqrt(abs(tempimg_bl2)),[]);title('blurred')
%% fiber
tempimg_bs_fiber0=bgsub(tempimg_bl2,8,0.2);

figure(200);subplot(1,2,2);imshow(sqrt(abs(tempimg_bs_fiber0)),[]);title('background subtracted (fiber)')
figure(300);subplot(1,2,1);histogram(tempimg_bs_fiber0(:),1000);title('fiber (histogram)')

fiber_bs=GetSeris_bg_bin(tempimg_bs_fiber0,1000);tempimg_bs_fiber=tempimg_bs_fiber0-fiber_bs;

figure(300);subplot(1,2,2);histogram(tempimg_bs_fiber(:),1000);title('corrected')
tempfiber=[tempfiber;sum(tempimg_bs_fiber(:))];
%% all signals
tempimg_bs_all0=bgsub(tempimg_bl2,128,0.01);
figure(250);subplot(1,2,1);imshow(sqrt(abs(tempimg_bl2)),[]);title('blurred')
```


doi:10.6342/NTU202303790

figure(250);subplot(1,2,2);imshow(sqrt(abs(tempimg_bs_all0)),[]);title('background subtracted (all)')

figure(400);subplot(1,2,1);histogram(tempimg_bs_all0(:),1000);title('all (histogram)')

all_bs=GetSeris_bg_bin(tempimg_bs_all0,1000);tempimg_bs_all=tempimg_bs_all0-all_bs;

figure(400);subplot(1,2,2);histogram(tempimg_bs_all(:),1000);title('corrected')

tempall=[tempall;sum(tempimg_bs_all(:))];

%%

tempimg_bs2=bgsub(tempimg_bl2,16*nucr,0);

[~,~,bga]=ThreshImage(tempimg_bs2);smaimg_max=smaimg_max-bga;

%tempmtx(rows,cols)=sum(sum(smaimg))/sum(sum(nucimg));

tempmtx_s_t1=sum(tempimg_bs2,'all');

tempmtx_s_t2=[tempmtx_s_t2;tempmtx_s_t1];

doi:10.6342/NTU202303790

```
%tempmtx_d(row,col)=sum(sum(tempimg_bs));

%tempmtx=tempmtx_s./tempmtx_d;

%nuc mask

tempimg_mk1=getdapimask(tempimg_bs-min(tempimg_bs(:))+0.01,nucr);


tempimg_gr=imadjust(mat2gray(tempimg_bs));th=graythresh(tempimg_gr(tempimg_gr
<=1 & tempimg_gr>=0));

tempimg_mk2=im2bw(tempimg_gr,th);

tempimg_mk=tempimg_mk1&tempimg_mk2;


tempimg_mk_sm=bwlabel(bwareaopen(logical(tempimg_mk),1*round(nucr^2)));

nucimg_ex=imdilate(tempimg_mk_sm,strel('disk',nucr),0);

nucimg_rg=nucimg_ex-tempimg_mk_sm;

%getinfo

nuc_info=regionprops((tempimg_mk_sm),'Centroid','Area','PixelIdxList');

cellnum=size(nuc_info,1);

tempmtx_n=zeros(cellnum,5);

for cc=1:cellnum
```


doi:10.6342/NTU202303790

```
            tempmtx_n(cc,1:2)=nuc_info(cc).Centroid;
            tempmtx_n(cc,3)=mean(tempimg_bs(nuc_info(cc).PixelIdxList));
            tempmtx_n(cc,4)=nuc_info(cc).Area;
        end
        %wellden(row,col)=size(tempmtx_n,1);
        wellden_t1=size(tempmtx_n,1);
        wellden_t2=[wellden_t2;wellden_t1]
        %%
        figure(100);subplot(1,2,1);hold on
        plot(tempmtx_n(:,1),tempmtx_n(:,2),'.r')
        %%
        toc
    end
    tempmtx_fiber=[tempmtx_fiber;tempfiber];
    tempmtx_all=[tempmtx_all;tempall];
    tempmtx_s=[tempmtx_s;tempmtx_s_t2]
    wellden=[wellden;wellden_t2]
end
```


doi:10.6342/NTU202303790

```
save([cwd,'celldata\wellsss.mat'],'tempmtx_s')

save([cwd,'celldata\','wellden.mat'],'wellden')

%

xlswrite('wellsss.xlsx',{'group_name'},1,'A1');

xlswrite('wellsss.xlsx',group_name,1,'A2');

xlswrite('wellsss.xlsx',{'tempmtx_s'},1,'B1');

xlswrite('wellsss.xlsx',tempmtx_s,1,'B2');

xlswrite('wellsss.xlsx',{'tempmtx_fiber'},1,'C1');

xlswrite('wellsss.xlsx',tempmtx_fiber,1,'C2');

xlswrite('wellsss.xlsx',{'tempmtx_all'},1,'D1');

xlswrite('wellsss.xlsx',tempmtx_all,1,'D2');

xlswrite('wellsss.xlsx',{'wellden'},1,'E1');

xlswrite('wellsss.xlsx',wellden,1,'E2');



%% cross

% tempmtx0=zeros(8,12);tempmtx0(2:4,:)=tempmtx(2:4,:);

% tempmtx0(5:7,3:10)=[tempmtx(5:7,7:10),tempmtx(5:7,3:6)];

%%
```


doi:10.6342/NTU202303790

```
% cmap=[0,0,0;jet(64)];

% figure(16);subplot(2,1,1)

% imagesc(tempmtx);colormap(cmap);colorbar;axis image

% set(gcf,'color','w')8

% set(gca,'xtick',1:12,'ytick',1:8,'yticklabel',char(65:72)')

% title('SMA Intensity (A.U.)');xlabel('Column#');ylabel('Row#')

% figure(16);subplot(2,1,2)

% y=[mean(tempmtx0(2:7,3:10))];

% %std=[std(tempmtx0(2:7,3:10))];

% hold off;bar(1:8,y,'white')

% hold on;errorbar(mean(tempmtx0(2:7,3:10)),std(tempmtx0(2:7,3:10))/sqrt(6),'.k')

% set(gca,'xtick',1:8,'xticklabel',num2str((3:10)'));xlabel('Column#')

% ylabel('SMA Intensity (A.U.)')

%%

% bb=smaimg_max(aa);

% figure;imshow(aa)

% bgn

% [~,~,bga]=ThreshImage(tempimg_bs2);
```


doi:10.6342/NTU202303790

```
% bga

% figure;histogram(tempimg_bs2,100)

% figure;histogram(tempimg_bs2,1000)

% aa=tempimg_bs2>2000;

% figure;imshow(aa)

% left=min(tempimg_bs2(:))

% bb=aa-left;

% threhold=aa+3*bb;

% threhold=aa+3*bb

% bb=bga-left;

% threshold=bga+3*bb

% threshold=bga+10*bb

% threshold=bga+15*bb

% aa=tempimg_bs2>threshold;

% figure;imshow(aa)

% threshold2=bga+1*bb

% lo=tempimg_bs2>threshold2 & tempimg_bs2<threshold;

% aa2=tempimg_bs2(lo)
```


doi:10.6342/NTU202303790

```
% aa2=tempimg_bs2(lo);

% figure;imshow(aa2,[])

% lo=tempimg_bs2>threshold2 & tempimg_bs2<threshold;

% lo1=tempimg_bs2>threshold2;

% open lo1

% aa2=tempimg_bs2*lo;

% figure;imshow(aa2,[])

% threshold2=bga+1*bb;

% threshold2=bga+1*bb

% threshold2=bga+0.5*bb

% lo1=tempimg_bs2>threshold2;

% aa2=tempimg_bs2*lo;

% figure;imshow(aa2,[])

% threshold2=bga;

% lo=tempimg_bs2>threshold2 & tempimg_bs2<threshold;

% aa2=tempimg_bs2*lo;

% figure;imshow(aa2,[])

% figure;imshow(lo,[])
```


doi:10.6342/NTU202303790

```
% threshold2=bga+0.5*bb;

% lo=tempimg_bs2>threshold2 & tempimg_bs2<threshold;

% figure;imshow(lo,[])

% aa2=tempimg_bs2*lo;

% aa2=tempimg_bs2.*lo;

% figure;imshow(aa2,[])

% threshold=bga+18*bb

% lo=tempimg_bs2>threshold2 & tempimg_bs2<threshold;

% figure;imshow(lo,[])

% figure;imshow(aa2,[])
```


doi:10.6342/NTU202303790

ORO_lipid_droplet_Factin_script_ncratio_20230516

(Fluro correction for actin quatification)

```
%%
close all;clc;clear mex
cwd='E:\20230605_HS68_KDFGFR1_TGFb_FGFRi_3days_Factin\shFGFR1\TIF\';cd
(cwd)
cfolder='';
%% fluo reference
c1_off=single(imresize(imread([cwd,'fluo_reference\DAPI_off.tif']),1));
c1_on=single(imresize(imread([cwd,'fluo_reference\DAPI_on.tif']),1));
c2_off=single(imresize(imread([cwd,'fluo_reference\TxRed_off.tif']),1));
c2_on=single(imresize(imread([cwd,'fluo_reference\TxRed_on.tif']),1));
%c3_off=single(imresize(imread([cwd,'fluo_reference\TxRed_off.tif']),1));
%c3_on=single(imresize(imread([cwd,'fluo_reference\TxRed_on.tif']),1));
c1_ref=c1_on-c1_off;c2_ref=c2_on-c2_off;
%c3_ref=c3_on-c3_off;
c1_mean=mean(c1_ref(:));c2_mean=mean(c2_ref(:));
%c3_mean=mean(c3_ref(:));
```


doi:10.6342/NTU202303790

```
%% correct image
chname={['c1'],['c2'],['c3']};chnum=size(chname,2);
cfile1=dir([cwd,'/',cfolder,'/','*',chname{1},'.tif']);
cfile2=dir([cwd,'/',cfolder,'/','*',chname{2},'.tif']);
%cfile3=dir([cwd,'/',cfolder,'/','*',chname{3},'.tif']);
%% correct c1img
filenum=size(cfile1,1);
for f=1:filenum
    %
    c1image=single(imread([cwd,'/',cfolder,'/',cfile1(f).name]));
    c1image_cr=(c1image-c1_off)./c1_ref*c1_mean+c1_off;
    c2image=single(imresize(imread([cwd,cfolder,'/',cfile2(f).name]),1));
    c2image_cr=(c2image-c2_off)./c2_ref*c2_mean+c2_off;
    %c3image=single(imread([cwd,cfolder,'/',cfile3(f).name]));
    %c3image_cr=(c3image-c3_off)./c3_ref*c3_mean+c3_off;
    %
    if f==1
        mkdir([cwd,cfolder,'\','fluo_corrected\'])
```


doi:10.6342/NTU202303790

```
        c1scale=prctile(c1image_cr(:),[0.1 99.9]);
        c2scale=prctile(c2image_cr(:),[0.1 99.9]);
        %c3scale=prctile(c3image_cr(:),[0.1 99.9]);
    end
    %% demo fluo_corrected image
    figure(11);set(gcf,'position',get(0,'ScreenSize'))
    figure(11);hold
off;subplot(2,3,1);imagesc(c1image);title(['Frame',num2str(f)]);ylabel('non-corrected')
    hold off;subplot(2,3,4);imagesc(c1image_cr,c1scale);title('ch1');ylabel('corrected')
    figure(11);hold off;subplot(2,3,2);imagesc(c2image);title(f);
    hold off;subplot(2,3,5);imagesc(c2image_cr);title('ch2');
    %figure(11);hold off;subplot(2,3,3);imagesc(c3image);title(f);
    %hold off;subplot(2,3,6);imagesc(c3image_cr,c3scale);title('ch3');
    %% save image
    imwrite(uint16(c1image_cr),[cwd,cfolder,'/','fluo_corrected/',cfile1(f).name]);
    imwrite(uint16(c2image_cr),[cwd,cfolder,'/','fluo_corrected/',cfile2(f).name]);
    %imwrite(uint16(c3image_cr),[cwd,cfolder,'/','fluo_corrected/',cfile3(f).name]);
end
```


doi:10.6342/NTU202303790

F-actin and stress fiber quantification

```
%%
clear;clc;close all
cwd='E:\20230605 HS68 KDFGFR1 TGFb FGFRi 3days Factin\shFGFR1\TIF\';
%%
for rows=2
    rowname=char(rows+64);
    for cols=7
        colname=['0',num2str(cols)];colname=colname(end-1:end);
        wellname=[rowname, colname];
        imgfolder=[cwd,'/fluo_corrected/'];
        % cd(imgfolder)
        nucr=17; % radius of nucleus
        oilr=34; % radius of cell
        toplength=nucr*4;

        %%
        for sitenum=1
```


doi:10.6342/NTU202303790

```
dispname=[wellname,' ',num2str(sitenum)];disp(dispname)
dapidir=dir([imgfolder,wellname,'*XY',num2str(sitenum),'*C1*.tif']);
oilrdir=dir([imgfolder,wellname,'*XY',num2str(sitenum),'*C2*.tif']);
zstacknum=size(dapidir,1); %it's Z stack number
%% image stack processing
for zzz=1:zstacknum
    tempdapi=single(imread([imgfolder,dapidir(zzz).name]));
    tempoilr=single(imread([imgfolder,oilrdir(zzz).name]));
    if zzz==1
        dapistack=zeros([size(tempdapi),zstacknum]);
        oilrstack=zeros([size(tempoilr),zstacknum]);
    end
    dapistack(:,:,zzz)=tempdapi;
    oilrstack(:,:,zzz)=tempoilr;
end
dapistack_sort=sort(dapistack,3,'descend');
oilrstack_sort=sort(oilrstack,3,'descend');
dapiimg=single(mean(dapistack_sort(:,:,1:3),3));
```


doi:10.6342/NTU202303790

```
oilrimg=single(mean(oilrstack_sort(:,:,1:3),3));

% demo original images


figure(100);subplot(1,3,1);imshow(dapiimg,[]);title(dispname);xlabel('DAPI')

figure(100);subplot(1,3,2);imshow(oilrimg,[]);xlabel('F-actin')

figure(100);subplot(1,3,3);imshowc(oilrimg,0,dapiimg,1);title('original
image')


%% background subtraction

dapiimg_bs=bgsub(dapiimg,4*nucr,0);

%oilrimg_bs=bgsub(oilrimg,4*oilr,0.2);

oilrimg_bs=bgsub(oilrimg,8*oilr,0.01);


figure(200);subplot(1,3,1);imshow(dapiimg_bs,[]);title(dispname);xlabel('DAPI')

figure(200);subplot(1,3,2);imshow(oilrimg_bs,[]);xlabel('F-actin')

figure(200);subplot(1,3,3);imshowc(oilrimg_bs,0,dapiimg_bs,1);title('background-
subtracted')
```


doi:10.6342/NTU202303790

```
%% oil red image correction
% oilrbg=GetSeris_bg_bin(oilrimg_bs,200); % correct bg to 0
oilrbg=0; % bg correction not performed
oilrimg_c=oilrimg_bs-oilrbg;
%% use dapi to get masks
dapiimg_mk0=getdapimask(sqrt(abs(dapiimg_bs)),nucr);
dapiimg_gr=mat2gray(dapiimg_bs);
gth=graythresh(dapiimg_gr);
dapiimg_mk2=imbinarize(dapiimg_gr,gth);
dapiimg_mk=bwareaopen(dapiimg_mk0 & dapiimg_mk2,1*nucr^2);

figure(240);subplot(1,3,1);imshow(dapiimg_bs,[]);title(dispname);xlabel('DAPI')
figure(240);subplot(1,3,2);imshow(dapiimg_mk,[]);xlabel('Mask')

figure(240);subplot(1,3,3);imshowc(dapiimg_mk,0,dapiimg_bs,1);title('Mask-DAPI')

%% rink mask
dapiimg_label=bwlabel(dapiimg_mk);
```


doi:10.6342/NTU202303790

```
dapiimg_label_dilate1=imdilate(dapiimg_label,strel('disk',round(nucr/2),0));
                dapiimg_label_dilate2=imdilate(dapiimg_label,strel('disk',nucr,0));
 %              dapiimg_ring=dapiimg_label_dilate-dapiimg_label; (NO excluding area)
                dapiimg_ring=dapiimg_label_dilate2-dapiimg_label_dilate1;

figure(270);subplot(1,3,1);imshow(dapiimg_bs,[]);title(dispname);xlabel('DAPI')
figure(270);subplot(1,3,2);imshowc(oilrimg_bs,0,dapiimg_bs,1);xlabel('DAPI-F-actin')
figure(270);subplot(1,3,3);imshowc(oilrimg_bs,dapiimg_ring>0,dapiimg_bs,1);title('rin
g mask')
                %% watershed mask
                dapiimg_bwdist=bwdist(dapiimg_mk);
                dapiimg_watershed=watershed(dapiimg_bwdist);

figure(300);subplot(1,2,1);imshowc(oilrimg_c,0,dapiimg_mk,1);title(dispname)
figure(300);subplot(1,2,2);imshowc(oilrimg_c,dapiimg_watershed==0,dapiimg_mk,1);t
itle('+ watershed')
```


doi:10.6342/NTU202303790

```
        %% prepare for data retrival by regionprops
        dapi_nuc=regionprops(dapiimg_mk,'centroid','area','pixelidxlist');
        dapi_ring=regionprops(dapiimg_ring,'area','pixelidxlist');
        dapi_watershed=regionprops(dapiimg_watershed,'area','pixelidxlist');
        nuc_num=size(dapi_nuc,1);
        nucmtx=zeros(nuc_num,12);
        %%
% 1x 2y 3nuc_area 4nuc_DAPI_avg_intensity
% 5nuc_ASMA_avg_intensity 6nuc_ASMA_top_intensity
% 7ring_area 8ring_avg_intensity 9ring_top_intensity
% 10watershed_area 11watershed_all_intensity 12watershed_top_intensity

        %% get information, cell by cell
        for nnn=1:nuc_num
            %% nuc info
            nucmtx(nnn,1:2)=dapi_nuc(nnn).Centroid;
            nucmtx(nnn,3)=dapi_nuc(nnn).Area;
            nucmtx(nnn,4)=mean(dapiimg_bs(dapi_nuc(nnn).PixelIdxList));
```


doi:10.6342/NTU202303790

```
                %% nuc YAP signals

tempnuc_list=sort(oilrimg_c(dapi_nuc(nnn).PixelIdxList),'descend');

                nucmtx(nnn,5)=mean(tempnuc_list);

                nucmtx(nnn,6)=trimmean(tempnuc_list(1:toplength),50);

                %% ring info & ring YAP signals

                nucmtx(nnn,7)=dapi_ring(nnn).Area;


tempring_list=sort(oilrimg_c(dapi_ring(nnn).PixelIdxList),'descend');

                nucmtx(nnn,8)=mean(tempring_list);

                nucmtx(nnn,9)=trimmean(tempring_list(1:toplength),50);

                %% watershed info

                nucmtx(nnn,10)=dapi_watershed(nnn).Area;


tempwatershed_list=sort(oilrimg_c(dapi_watershed(nnn).PixelIdxList),'descend');

                nucmtx(nnn,11)=sum(tempwatershed_list);

                nucmtx(nnn,12)=trimmean(tempwatershed_list(1:toplength),50);

            end
```


doi:10.6342/NTU202303790

```
%% demo nuc avg

figure(360);imshowc(oilrimg_bs,0,sqrt(abs(dapiimg_bs)),1);xlabel('DAPI-F-actin')
hold on;plot(nucmtx(:,1),nucmtx(:,2),'.w')
text(nucmtx(:,1),nucmtx(:,2),num2str(round(nucmtx(:,5))),'color','w')
title([dispname,' F-actin nuc avg'])
%% demo nuc top

figure(380);imshowc(oilrimg_bs,0,sqrt(abs(dapiimg_bs)),1);xlabel('DAPI-F-actin')
hold on;plot(nucmtx(:,1),nucmtx(:,2),'.w')
text(nucmtx(:,1),nucmtx(:,2),num2str(round(nucmtx(:,6))),'color','w')
title([dispname,' F-actin nuc top'])

%% demo ring avg

figure(400);imshowc(oilrimg_bs,0,sqrt(abs(dapiimg_bs)),1);xlabel('DAPI-F-actin')
hold on;plot(nucmtx(:,1),nucmtx(:,2),'.w')
text(nucmtx(:,1),nucmtx(:,2),num2str(round(nucmtx(:,8))),'color','w')
```


doi:10.6342/NTU202303790

```
title([dispname,' F-actin ring avg'])

%% demo ring top

figure(420);imshowc(oilrimg_bs,0,sqrt(abs(dapiimg_bs)),1);xlabel('DAPI-F-actin')

hold on;plot(nucmtx(:,1),nucmtx(:,2),'.w')

text(nucmtx(:,1),nucmtx(:,2),num2str(round(nucmtx(:,9))),'color','w')

title([dispname,' F-actin ring top'])

%% demo watershed all

figure(440);imshowc(oilrimg_bs,dapiimg_watershed==0,sqrt(abs(dapiimg_bs)),1);xlabe
l('DAPI-F-actin')

hold on;plot(nucmtx(:,1),nucmtx(:,2),'.w')

text(nucmtx(:,1),nucmtx(:,2),num2str(round(nucmtx(:,11))),'color','w')

title([dispname,' F-actin watershed all'])

%% demo watershed top
```


doi:10.6342/NTU202303790

```
figure(460);imshowc(oilrimg_bs,dapiimg_watershed==0,sqrt(abs(dapiimg_bs)),1);xlabe
l('DAPI-F-actin')
                hold on;plot(nucmtx(:,1),nucmtx(:,2),'.w')
                text(nucmtx(:,1),nucmtx(:,2),num2str(round(nucmtx(:,12))),'color','w')
                title([dispname,' F-actin watershed top'])
               %% bigmax=max([nucmtx(:,5);nucmtx(:,8)]);
               figure(480);

subplot(1,2,1);plot(nucmtx(:,8),nucmtx(:,5),'.');axis([0,bigmax,0,bigmax])
                hold on;plot([0,bigmax],[0,bigmax],':k')
                xlabel('Cytosol');ylabel('Nucleus');title(['F-actin ',dispname])
                subplot(1,2,2);plot(nucmtx(:,8),nucmtx(:,5),'.');axis([0,5000,0,5000])
                hold on;plot([0,5000],[0,5000],':k')
                xlabel('Cytosol');ylabel('Nucleus');title(['F-actin ',dispname])
                %%
                save([imgfolder,wellname,'_XY',num2str(sitenum)],'nucmtx')
            end
```


doi:10.6342/NTU202303790

```
        end

end
```


doi:10.6342/NTU202303790